Evolution of an Impact-Generated H_2O–CO_2 Atmosphere and Formation of a Hot Proto-Ocean on Earth

YUTAKA ABE AND TAKAFUMI MATSUI

Geophysical Institute, Faculty of Science, University of Tokyo, Bunkyo-ku, Tokyo, Japan

(Manuscript received 26 February 1987, in final form 25 April 1988)

ABSTRACT

Due to impact degassing during accretion, a hot H_2O-rich proto-atmosphere was possibly formed on the growing Earth. We investigate the evolution of an impact-generated H_2O–CO_2 atmosphere at the final stage of accretion by using a one-dimensional radiative-convective atmosphere model. Since atmospheric pressure is high (~200 bar) and close to the critical point of water vapor (647 K, 220 bar), we need to take into account the nonideal behavior of gases in the calculation. It is shown that the surface temperature suddenly decreases when the impact (accretion) energy flux decreases to about 150 W m^{-2}, and that a proto-ocean is formed on the growing Earth. The estimated temperature of a proto-ocean is consistent with that of an archaean ocean estimated from the oxygen isotope data.

1. Introduction

High velocity impacts of planetesimals into the growing Earth have been considered to occur during accretion, which results in degassing of volatiles contained in the Earth forming planetesimals. Recently, such an impact degassing and formation of an impact-induced atmosphere during accretion has been extensively studied experimentally (Boslough et al. 1980, 1982; Lange and Ahrens 1982b, 1984, 1986) and theoretically (Jakosky and Ahrens 1979; Lange and Ahrens 1982a; Abe and Matsui 1985, 1986; Matsui and Abe 1986a,b).

Judging from the volatile abundance in meteorites and the terrestrial hydrosphere, water vapor is a main composition of an impact-generated atmosphere. If such an H_2O-rich proto-atmosphere was formed, the gravitational energy released during accretion cannot directly escape into interplanetary space, and thus the surface of the growing Earth is heated up. This is because H_2O absorbs the infrared radiation efficiently. Owing to such a blanketing effect of the proto-atmosphere, the surface of the growing Earth melts, and a magma ocean is formed (Abe and Matsui, 1985, 1986; Matsui and Abe, 1986a,b). Once a magma ocean covered the entire surface of the growing Earth, the surface temperature and mass of H_2O in the atmosphere are shown to be kept nearly constant during accretion (Abe and Matsui 1986; Matsui and Abe 1986b). This is because the mass of H_2O in the atmosphere is controlled by dissolution of H_2O in silicate melt: when the surface temperature is between the solidus and liquidus temperatures, the amount of water dissolved into a magma ocean increases with increasing surface temperature because of an increase in degree of partial melting, which results in a decrease of H_2O in the atmosphere. A decrease of H_2O in the atmosphere lowers the efficiency of the blanketing effect; thus, the surface temperature decreases. Such a negative feedback keeps the surface temperature and mass of H_2O in the atmosphere nearly constant.

The total mass of H_2O in an impact-induced atmosphere at the end of accretion is shown to be about $\sim 10^{21}$ kg, which is very close to the mass of the present hydrosphere of the Earth (about 1.4×10^{21} kg). The final mass of the atmosphere is insensitive to variations in the input parameter values, such as accretion time, initial water content of planetesimals and the efficiency of impact-degassing at low temperature (Abe and Matsui 1986; Matsui and Abe 1986b). This is namely due to the self-regulation processes mentioned before. These results seem to suggest an impact-origin of the Earth's hydrosphere during accretion. Of course, this satisfies the secondary origin constraints of the terrestrial atmosphere given by the rare gas data (Brown 1952; Hamano and Ozima 1978).

During the middle stage of accretion, the main heat source of the atmosphere is the impact energy flux given at the base of the atmosphere. However, the impact energy flux rapidly decreases at the late stage of accretion, because the accretion rate slows down. Then the solar flux surpasses the impact energy flux at the end of accretion. Being accompanied with such a change

Corresponding author address: Dr. Yutaka Abe, Geophysical Institute, Faculty of Science, University of Tokyo, Bunkyo-ku, Tokyo 113, Japan.

in heat source of the atmosphere, the surface temperature decrease and a hot proto-ocean is possibly formed on the Earth (Matsui and Abe 1986c).

In the previous studies, however, we have made a number of simplifications in calculating the atmospheric structure. In particular, the following effects were ignored: 1) condensation of H_2O in the atmosphere; 2) nonideal behaviors of H_2O at high pressure; 3) wavelength, pressure, temperature and pathlength dependences of the absorption coefficient; 4) greenhouse effect; 5) Rayleigh scattering at short wavelength; and 6) geometrical effect (sphericity) of the atmosphere on the radiative transfer. (The greenhouse effect was taken into account only in Matsui and Abe (1986c).) In addition to these simplifications, our treatment of convection was very rough in the previous studies. In this study, therefore, we take into account all of these effects and try to make a one-dimensional radiative-convective model of a proto-atmosphere to discuss its evolution more rigorously.

We consider a change in the atmospheric structure with decreasing impact energy flux at the last stage of accretion. It should be noted that the temperature structure of the atmosphere heated from below is different from that heated by solar radiation; if the atmosphere is heated by solar radiation, the net upward energy flux is not constant in the atmosphere due to absorption of solar radiation in the atmosphere. To the contrary, if the atmosphere is heated from below, the net upward energy flux is constant throughout the atmosphere. Hence, the change in the atmospheric structure caused by changing the impact energy flux is different from that caused by changing the solar flux. In this respect, this study is completely different from those related to the runaway greenhouse of Venus (e.g., Pollack 1971; Kasting et al. 1984), which considered the change in the atmospheric structure caused by increasing the solar flux.

2. Method

To take into account the effect of condensation and wet-convection properly, at least two gas components are required. Hence, we consider an atmosphere composed of H_2O and CO_2, because CO_2 is the second most abundant component in the Earth's volatile budget (Poldervaart 1955).

We use a radiative–convective atmosphere model to calculate the atmospheric structure. The radiative–convective model is based on a steady state method, which uses a Newton iteration process to achieve convergence. The atmosphere is divided into two layers, radiative (or stratosphere) and convective (or troposphere). The radiative layer is assumed to be in radiative equilibrium. The temperature gradient in the convective layer, which is in convective equilibrium, is assumed to be equal to the adiabatic one. The boundary between these two regions, i.e., the tropopause, is moved up or down as individual layers become convectively stable or unstable. (We divided the atmosphere into 50 uneven layers to calculate the atmospheric structure.) This method is only slightly different from that used by Kasting et al. (1984). See appendix A for more detail.

a. *Convective lapse rate*

The temperature gradient in a convective layer is assumed to be equal to the adiabatic gradient. In the following we discuss the adiabatic gradient of nonideal gas, since the critical point of water vapor (647 K and 2.2×10^7 Pa) is close to the temperature-pressure range considered in this study. If we assume an ideal gas, the relative error will exceed 100%. In addition, we may not ignore the temperature dependence of specific heat under such a high temperature condition as considered in this study.

In general, the wet-adiabat of a nonideal gas mixture is given by (see appendix B for derivation),

$$\left(\frac{\partial T}{\partial P}\right)_s = \frac{S_n G_P - S_P G_n}{S_T G_n - S_n G_T} \quad (wet) \tag{1}$$

$$\left(\frac{\partial x_v}{\partial P}\right)_s = (1 - x_v)\frac{S_P G_T - S_T G_P}{S_T G_n - S_n G_T} \quad (wet) \tag{2}$$

with

$$G_T = -\left\{R \ln x_v + \int_0^P \left[\left(\frac{\partial v_v}{\partial T}\right) - \left(\frac{\partial v_v^*}{\partial T}\right)\right]dP' + \frac{\partial}{\partial T}\int_{P^*(T)}^P (v_v^* - v_c^*)dP'\right\} \tag{3a}$$

$$G_P = -(v_v - v_c^*) \tag{3b}$$

$$G_n = -\left\{RT\left(\frac{1}{x_v} - 1\right) + \int_0^P \left[(1 - x_v)\frac{\partial v_v}{\partial x_v} - \sum_i x_i \frac{\partial v_i}{\partial x_i}\right]dP'\right\} \tag{3c}$$

$$S_T = \frac{C_{pg}(P, T)}{T} + x_c\left\{\frac{C_{pv}(P, T)}{T} - 2\left[\left(\frac{\partial v_v^*}{\partial T}\right) - \left(\frac{\partial v_c^*}{\partial T}\right)\right]_{P^*(T)}\frac{dP^*(T)}{dT} - (v_v^* - v_c^*)_{P^*(T)}\frac{d^2P^*(T)}{dT^2} + \int_{P^*(T)}^P \left(\frac{\partial^2 v_c^*}{\partial T^2}\right)dP'\right\} \tag{4a}$$

$$S_P = -\left[\left(\frac{\partial v_g}{\partial T}\right)_P + x_c\left(\frac{\partial v_c^*}{\partial T}\right)_P\right] \tag{4b}$$

$$S_n = -\left\{R \ln x_v + \int_0^P \left[\left(\frac{\partial v_v}{\partial T}\right) - \left(\frac{\partial v_v^*}{\partial T}\right)\right] dP' + \frac{\partial}{\partial T}\int_{P^*(T)}^P (v_v^* - v_c^*) dP'\right\} \quad (4c)$$

where x_v is the mole fraction of H_2O in the vapor phase ($=X_{H_2O}$), and v_v, v_v^* and v_c^* are the partial molar volume of water vapor, and molar volumes of pure water vapor and cloud particles (liquid or ice), respectively. (For the case of a nonideal gas mixture, v_v and v_v^* are different usually, which implies that Dalton's law on partial pressure does not hold any more.) Here $P^*(T)$ is the saturation vapor pressure of pure water vapor at temperature T, and R is the gas constant. In the derivation of Eqs. (1) and (2), we only assumed that 1) the entropy of the gas-cloud particle mixture is given by the sum of that of the gas phase and cloud particles, 2) cloud particles are composed of pure H_2O, and 3) cloud particles are equilibrated with gas phase. Since no additivity of entropy within gas phase is assumed, these expressions are more general than those given by Ingersoll (1969).

Equations (1) and (2) are valid only where cloud particles exist. We call such a region the wet convective layer. Cloud particles exist only when the following condition is satisfied:

$$\Delta g(P, T, x_v) \equiv -RT \ln x_v - \int_0^P (v_v - v_v^*) dP' - \int_{P^*(T)}^P (v_v^* - v_c^*) dP' = 0. \quad (5)$$

This is the equilibrium condition between cloud particles and water vapor.

When $\Delta g(P, T, x_v) > 0$ for given P, T and x_v, the atmosphere contains no cloud particles, i.e., it is a dry layer. In the dry layer the adiabatic gradient is given by

$$\left(\frac{\partial T}{\partial P}\right)_s = -\frac{S'_P}{S'_T} \quad (dry) \quad (6)$$

with

$$S'_T = \frac{C_{pg}(P, T)}{T} \quad (7a)$$

$$S'_P = -\left(\frac{\partial v}{\partial T}\right)_p. \quad (7b)$$

The convective layer where no condensation occurs is henceforth called the dry convective layer.

Given the heat capacity, equation of state, and saturation vapor pressure, we can calculate the adiabatic temperature gradient using the above equations. As an equation of state of fluid we use that proposed by Peng and Robinson (1976). (Ice is assumed to be incompressible.) The Peng–Robinson equation of state is one of the modifications of the van der Waals' equation and is given by

$$P = \frac{RT}{v - b} - \frac{a(T)}{v^2 + 2bv - b^2} \quad (8)$$

where v is the molar volume of fluid. Here $a(T)$ and b are defined, respectively, by

$$a(T) \equiv \sum_i \sum_j x_i x_j (1 - k_{ij}) \sqrt{a_i a_j} \times [1 + c_i(1 - \sqrt{T/T_{ci}})] \times [1 + c_j(1 - \sqrt{T/T_{cj}})] \quad (9a)$$

$$b \equiv \sum_i x_i b_i \quad (9b)$$

$$a_i \equiv 0.45724 \frac{R^2 T_{ci}^2}{P_{ci}} \quad (9c)$$

$$b_i \equiv 0.07780 \frac{RT_{ci}}{P_{ci}} \quad (9d)$$

$$c_i \equiv 0.37464 + 1.54226\omega_i + 0.26992\omega_i^2 \quad (9e)$$

where T_{ci} and P_{ci} are the temperature and pressure at the critical point of gas component i, respectively; ω_i is an acentric factor of gas component i; and k_{ij} is the binary interaction coefficient which characterizes a binary formed by component i and j and can be empirically determined. Numerical constants in these equations are universal constants derived by Peng and Robinson (1976) by using the theory of corresponding states. For the case of H_2O, the pressure calculated from the Peng–Robinson equation for a given molar volume is very close to the values listed in a steam table (Keenan et al. 1978). The difference is within ~3% even along the saturation curve of water vapor. Such a correspondence is better than that of other modified van der Waals' equations of state. (As mentioned before, the equation of state for ideal gas results in the relative errors larger than 150% at the same condition.) Parameter values used in this study are summarized in Table 1.

Specific heat is given by

$$C_{pg}(P, T) = \sum_i^{\text{all}} x_i C_{pi0}^I(T) - T\int_0^P \left(\frac{\partial^2 v}{\partial T^2}\right)_{p'} dP' \quad (10a)$$

$$C_{pv}(P, T) = C_{pv0}^I(T) - T\int_0^P \left(\frac{\partial^2 v_v^*}{\partial T^2}\right)_{p'} dP' \quad (10b)$$

and C_{p0}^I is given by

$$C_{p0}^I(T) = C_1 + C_2 T + C_3 T^2 + C_4 T^3 \quad (11)$$

where C_1, C_2, C_3 and C_4 are the empirically determined constants. When we use the parameters shown in Table 1, an average error of this equation is about 0.25% at 273 K $\leq T \leq$ 1800 K (Hougen et al. 1959).

TABLE 1. Thermodynamical parameters used in this study. (Saito 1982; Hougen et al. 1959)

Species	P_c (10^5 Pa)	T_c (K)	Accentric factor	Constants for heat capacity calculation (J/mol·K)			
				C_1	C_2	C_3	C_4
H_2O	220.4	647.3	0.344	32.24	1.923×10^{-3}	1.055×10^{-5}	-3.511×10^{-9}
CO_2	73.76	304.2	0.225	22.26	5.981×10^{-2}	-3.501×10^{-5}	7.469×10^{-9}

$R = 8.3148$ J/mol·K.
$k_{ij} = 0$.

Following Eisenberg and Kauzmann (1969), we use the relations given by Osborne–Mayers and Washburn as the saturation vapor pressure of H_2O. At 268.15 K $\leqslant T \leqslant$ 647.26 K we use the Osborne-Mayers' formula. Then the saturation vapor pressure of H_2O over liquid water is given by

$$\ln P^*(T) = \alpha - \frac{\beta}{t} + \frac{\gamma x}{t}[\exp(\delta x^2) - 1] - \epsilon \exp(-\eta y) \quad (12a)$$

where $P^*(T)$ is in Pascals and

$$t = T(\mathrm{K}) + 0.01$$
$$x = t^2 - 293\,700$$
$$y = [647.26 - T(\mathrm{K})]^{5/4}$$
$$\alpha = 24.021415$$
$$\beta = 4616.9134$$
$$\gamma = 3.1934553 \times 10^{-4}$$
$$\delta = 2.7550431 \times 10^{-11}$$
$$\epsilon = 1.0246503 \times 10^{-2}$$
$$\eta = 1.3158813 \times 10^{-2}.$$

The saturation vapor pressure calculated from Eq. (12a) fits well the measured value within a relative error of 10^{-4} (Eisenberg and Kauzmann 1969).

The saturation vapor pressure over ice is given by the Washburn's equation

$$\ln P^*(T) = \alpha' - \frac{\beta'}{t} + \gamma' \ln t - \delta' t + \epsilon' t^2 \quad (12b)$$

where $P^*(T)$ is in Pascals and

$$t = T(\mathrm{K}) - 0.05$$
$$\alpha' = -10.666189$$
$$\beta' = 5631.1206$$
$$\gamma' = 18.953038$$
$$\delta' = 3.8614490 \times 10^{-2}$$
$$\epsilon' = 2.7749374 \times 10^{-5}.$$

b. Radiative transfer

Because of the high atmospheric temperature considered in this study, the spectral range of thermal radiation emitted from the atmosphere extends to short wavelengths. At the spectral range shorter than 1 μm, in particular the visible range, the molecular Rayleigh scattering is not negligible. However, we must take into account pathlength dependence of the absorption in the infrared region. It is difficult, however, to take into account the pathlength dependence of the absorption coefficient and scattering simultaneously. Hence, as done by Pollack (1971), we ignore the pathlength dependence of absorption in the spectral range where scattering is taken into account. Henceforth, we call such a spectral range the scattering band. In the infrared region, where scattering may be neglected, we take into account the pathlength dependence of absorption. Henceforth, we call these spectral ranges the nonscattering bands. We consider 47 nonscattering bands in the spectral range of 0–14 286 cm^{-1} and one scattering band in the spectral range of >14 286 cm^{-1}. We may consider that the nonscattering and scattering bands roughly correspond to the infrared and visible bands, respectively.

The radiant flux density in the nonscattering bands was calculated from the radiative transfer equation in a plane-parallel atmosphere. Since the optical thickness of the atmosphere is very large, we use a method similar to that used by Kasting et al. (1984) to calculate the radiant flux density (see appendix A for more detail). The effect of sphericity of the atmosphere was taken into account in calculation of the radiant flux from the radiant flux density. In the scattering band we use the two-stream approximation to calculate the radiative transfer by taking into account the sphericity of the atmosphere.

Unlike the usual radiative-convective atmosphere models, our model cannot treat the solar radiation and thermal radiation separately. This is because the wavelength range of the thermal radiation is overlapped with that of the solar radiation. The solar radiative transfer is calculated by using the same method as that for the thermal radiative transfer (see appendix A for more detail).

For simplicity the effect of cloud on the radiative transfer is ignored in this study. It may result in over-

estimation of the greenhouse effect, as will be discussed later.

1) LONG WAVELENGTH RADIATION (NON-SCATTERING BANDS)

In the nonscattering bands, we consider both the line absorption of H_2O and CO_2, and the continuum absorption of H_2O.

(i) Line absorption. In the present Earth's lower atmosphere, the line shape is approximated by the Lorentz line shape. At higher pressure, however, the line shape is known to deviate from the Lorentz line shape (e.g., Burch and Gryvnak 1966). At lower pressure, the line shape changes from the Lorentz line shape to the Doppler line shape because of decrease in collision frequency. At even lower pressure, the assumption of local thermodynamic equilibrium (LTE) may break down because of very low frequency of collision. The ratio between the relaxation time (due to collision) and the natural life time of excited state is estimated to be $\sim 10^{-10}$ for the rotation band and $\sim 10^{-4}$–10^{-5} for the vibration-rotation bands at standard temperature and pressure (Goody 1964). Since the relaxation time is considered to be inversely related to pressure, we may assume that LTE is satisfied up to about 0.1 mb level. In this study we consider only the region where atmospheric pressure is higher than 0.1 mb and thus we can assume LTE.

We also neglect a change in the line shape at high pressure, because, in the lower atmosphere where such an effect may be important, the atmosphere is convectively equilibrated in most of the cases considered in this study. We also neglect the temperature dependence of the line intensity and the hot band for the same reason.

As done by Kasting et al. (1984), we treat the transition of the line shape between the Lorentz and the Doppler one by using the Fels' (1979) approximation. Then we can take into account the effect of line shape transition when the Goody random model parameters, S/δ and $\pi\alpha_0/\delta$, and mean line spacing, δ, are all given. We use the δ value estimated by Kasting et al. (1984). The Goody random model parameters used in this study is shown in Table 2.

In the following, we briefly describe the data required for calculating the line absorption. For the rotation band and 6.3 μ band of H_2O and 15 μ band of CO_2 we use the Goody random model parameters compiled by Rodgers and Walshaw (1966). We also use band parameters of CO_2 tabulated by Houghton (1977). For the more shorter wavelength range, we used the total absorption data measured by Howard et al. (1956). Actually we used the parameters refitted by Roach (1961), which provides the absorption data for 3.2, 2.7, 1.87, 1.38, 1.1, and 0.94 μm bands of H_2O and 4.3, 2.7, 2.0, 1.6, and 1.4 μm bands of CO_2. Since these data are not parameterized for the Goody random model, we cannot take into account the effect of line shape transition for these absorption bands. For 0.81 and 0.7 μm bands of H_2O we estimate the Goody random model parameters based on the total absorption data reported by Fowle (1915). (See appendix C for more detail.)

Then we can estimate the line absorption data in the following wavenumber region: 0–2200, 2800–4400, 4800–5900, 6500–8000, 8300–9300, 10 100–11 500, 11 906–12 658, 13 514–14 286 cm^{-1} for H_2O, and 582–1200, 2160–2500, 3480–3800, 4750–5200, 6000–6550, and 9300–10 100 cm^{-1} for CO_2.

However there still remains some "window" regions where no absorption data are assigned to. Even if we take into account the continuum absorption by H_2O, no absorption data are assigned to the wavenumber region of 4400–4800, 5900–6000, 8000–8300, 9300–

TABLE 2. Random model parameters used in this study.

Gas	Wavenumber (cm^{-1})	S/δ ($cm^2\ g^{-1}$)	$\pi\alpha_{L0}/\delta$	Band number	Data source
H_2O	0–40	579.75	0.093	1	(1) (a)
	40–160	7210.3	0.182	2	(1) (a)
	160–280	6024.8	0.094	3	(1) (a)
	280–380	1614.1	0.081	4	(1) (a)
	380–500	139.03	0.080	5	(1) (a)
	500–600	21.64	0.068	6, 7	(1) (a)
	600–720	2.919	0.060	8	(1) (a)
	720–800	0.3856	0.059	9, 10	(1) (a)
	800–900	0.0715	0.067	11	(1) (a)
	1 200–1 350	12.65	0.089	14	(1) (a)
	1 350–1 450	134.4	0.230	15	(1) (a)
	1 450–1 550	632.9	0.320	16	(1) (a)
	1 550–1 650	331.2	0.296	17	(1) (a)
	1 650–1 750	434.1	0.452	18	(1) (a)
	1 750–1 850	136.0	0.359	19	(1) (a)
	1 850–1 950	35.65	0.165	20	(1) (a)
	1 950–2 050	9.015	0.104	21	(1) (a)
	2 050–2 200	1.529	0.116	22, 23	(1) (a)
	2 200–2 500	0.1604	0.1276	24	(2) (b)
	2 500–2 800	0.1112	0.1276	25	(2) (b)
	4 400–4 800	0.03806	0.1276	30, 31	(2) (b)
	5 900–6 000	0.01372	0.1276	34	(2) (b)
	6 000–6 500	0.03244	0.1276	35	(2) (b)
	8 000–8 300	0.007821	0.1276	36	(2) (b)
	9 300–10 100	0.004386	0.1276	42	(2) (b)
	11 500–11 906	0.002027	0.1276	44	(2) (b)
	11 906–12 658	0.0464	0.1276	45	(3) (c)
	12 658–13 514	0.001137	0.1276	46	(2) (b)
	13 514–14 286	0.0387	0.1276	47	(3) (c)
CO_2	380–500	0.0001451	0.2597	5	(4) (d)
	500–582	0.05164	0.1122	6	(4) (d)
	582–752	718.7	0.448	7, 8, 9	(1) (a)
	752–800	0.3591	0.6557	10	(4) (d)
	800–900	0.008146	0.5559	11	(4) (d)
	900–1 000	0.02054	0.2741	12	(4) (d)
	1 000–1 200	0.01425	0.1610	13	(4) (d)

(1) Rodgers and Walshaw (1966)
(2) estimated from the data of Ludwig (1971)
(3) estimated from the data of Fowle (1915)
(4) estimated from tabulated parameters of Houghton (1977)

10 100, 11 500–11 906 and 12 658–13 514 cm^{-1}. Since H_2O also shows absorption in these spectral ranges, neglection of absorption in these ranges results in a significant underestimation of opacity of the atmosphere. Hence, we must estimate the absorption data in these band gaps and more shorter wavelength. In this study we estimate the Goody random model parameters of these spectral ranges from the laboratory data compiled by Ferriso et al. (1966) and its revised version by Ludwig (1971). (See appendix C for more detail.) In the 2200–2800 cm^{-1} range, we take into account only the continuum absorption, but no line absorption parameters are estimated from the Ludwig's total absorption data.

(ii) Continuum absorption. It has been known that the continuum absorption of H_2O extends from at least ~250 to 2860 cm^{-1} (Bignell 1970). We took into account the continuum absorption in the spectral range of 280–2800 cm^{-1}. We use the column transmission function given by Roberts et al. (1976) to represent the continuum absorption of H_2O:

$$-\ln T_R = C_0(\nu) \exp\left[1800\left(\frac{1}{T} - \frac{1}{296}\right)\right] nw \quad (13)$$

where ν is the wavenumber, n and w are the number density of H_2O molecules and the pathlength of H_2O, respectively. For the 333–1250 cm^{-1} region

$$C_0 = 1.25 \times 10^{-22} + 1.67 \times 10^{-19} \exp(-7.87 \times 10^{-3}\nu) \quad (14)$$

where ν, n and w are measured in cm^{-1}, number of molecules per cubic centimeter and atm-centimeter, respectively (Roberts et al. (1976)). We use Eq. (13) for the region outside 333–1250 cm^{-1} (Kasting et al. (1984)). We extrapolate Eq. (14) down to 1550 cm^{-1}. Here C_0 is assumed to be 5×10^{-24} $cm^2/(mol \cdot atm)$ for the 1550–2800 cm^{-1} region, 1.2×10^{-20} $cm^2/(mol \cdot atm)$ for the 280–380 cm^{-1} region.

2) SHORT WAVELENGTH RADIATION (SCATTERING BAND)

We assume that the spectral range shorter than 14 286 cm^{-1} is the scattering band. A very weak absorption band of H_2O, which is called the "rain" band, exists in the region 14 225–17 483 cm^{-1} (Kondratyev 1969). Since no quantitative data existed in this range, we neglected this band and assumed that the albedo for single scattering is 1. It may result in overestimation of the transmission of solar radiation and the greenhouse effect. We use the nondimensional refractive index for Na-D line for simplicity (Allen 1963). Though the extinction coefficient is proportional to the fourth power of the wavenumber, we use 14 643 cm^{-1} throughout this scattering band. This treatment results in underestimation of the scattering and overestimation of the transmittance for the solar radiation; however, the relative error in transmittance is less than 3% in the case of thick atmosphere ($P_s > 5 \times 10^6$ Pa) considered in this study.

3. Results

Given the solar radiant flux density S_0, energy flux density given at the surface F_0, and two parameters at the base of the atmosphere, atmospheric pressure P_s, and mole fraction of H_2O, we can calculate the atmospheric structure. Here F_0 may be considered as an impact energy flux during accretion or heat flow from the interior after accretion. The variables P_s and X_{H_2O} at the base of the atmosphere are assumed to be 2×10^7 Pa (200 bars) and 0.9, respectively, as long as no condensation of H_2O occurs at the base of the atmosphere. Then the total H_2O and CO_2 masses in the atmosphere are $\sim 10^{21}$ and $\sim 2.5 \times 10^{20}$ kg, respectively. This CO_2 abundance corresponds to the present CO_2 budget in the near-surface layer of the Earth (Poldarvaart 1955). When condensation occurs at the base of the atmosphere, P_s is determined so that the total mass of CO_2 in the atmosphere may be close to 2.5×10^{20} kg. For the radius and mass of the planet, we use those of the present Earth, 6.378×10^6 m and 5.97×10^{24} kg, respectively. Then the atmospheric structure is determined as a function of the solar flux density, S_0, and heat flux density given at the base of the atmosphere, F_0. Model parameters and major results are summarized in Table 3.

a. Temperature profile

Figure 1 shows the temperature profile of the atmosphere for various values of F_0. The saturation curve of pure H_2O vapor is also shown in this figure. The solar radiation is assumed to be about 30% lower than the present value, 960 W m^{-2} for the proto-Earth (Ezer and Cameron 1965). It is shown that the temperature profile is mostly along the adiabat. It is also shown that the temperature gradients in the upper and middle atmosphere are very close to each other. This is because the adiabatic temperature gradient converges to the saturation curve of H_2O when condensation occurs in the atmosphere composed mainly of H_2O.

The difference between various atmospheric structure models becomes clear when we plot the vertical temperature profile on a temperature versus height diagram (Fig. 2). We can clearly see the difference in atmospheric structure with change in F_0 on this figure. When $F_0 > 150$ W m^{-2}, the lower atmosphere is dry (no condensation of H_2O occurs). Even if raindrops fall out from the upper wet layer, they are considered to evaporate before reaching the base of the atmosphere. Hence, no ocean could be formed for such a case. Vertical thickness of the dry-convective layer decreases with decreasing F_0, and the dry convective layer disappears at $F_0 \sim 150$ W m^{-2}. This means than condensation of H_2O is expected to occur at the base of

TABLE 3. Model parameters and major results.

Model	S_0 (W m^{-2})	F_0 (W m^{-2})	P_s (10^5 Pa)	X_{H_2O} At the cold trap	X_{H_2O} At the surface	T_s (K)	M_{H_2O} (kg)[a]	M_{CO_2} (kg)[a]
E0	960	0	50	2.8×10^{-8}	0.20	455.2	1.69×10^{19}	2.45×10^{20}
E50	960	50	50	2.8×10^{-8}	0.25	466.6	2.44×10^{19}	2.37×10^{20}
E100	960	100	50	6.8×10^{-6}	0.37	484.5	4.17×10^{19}	2.20×10^{20}
E150	960	150	90	0.38	0.73	570.0	2.22×10^{20}	2.52×10^{20}
E200	960	200	200	0.86	0.90	1545.0	8.50×10^{20}	2.31×10^{20}
E250	960	250	200	0.85	0.90	1652.0	8.52×10^{20}	2.31×10^{20}
E300	960	300	200	0.86	0.90	1712.0	8.53×10^{20}	2.32×10^{20}
V0[b]	1830	0	80	0.09	0.53	535.0	1.16×10^{20}	3.04×10^{20}

[a] Total mass in the atmosphere.
[b] V0 is a proto-Venusian atmosphere model.

the atmosphere at $F_0 < 150$ W m^{-2}. In other words, a proto-ocean is formed on the surface of the proto-Earth. It is clear, as shown in Figure 2, that the change in atmospheric structure with decreasing F_0 occurs fairly drastic only at $F_0 = \sim 150$ W m^{-2}. This change will be discussed in more detail later (Fig. 6).

The temperature profile in the convective layer is close to a straight line, but slightly curved. In addition, the lapse rate seems to differ between various models, which is ascribed to nonideal behavior of gases, temperature dependence of specific heat and variation in H_2O concentration. It is, then, suggested that we cannot assign a single lapse rate for the troposphere as done by Pollack (1971).

The height of tropopause is much higher than present. When $F_0 > 200$ W m^{-2}, the tropopause is located higher than 250 km above the ground. The height of atmosphere decreases with decreasing F_0. The tropopause is located at 40 km above the ground even for the case of $F_0 = 0$ W m^{-2} (model E0).

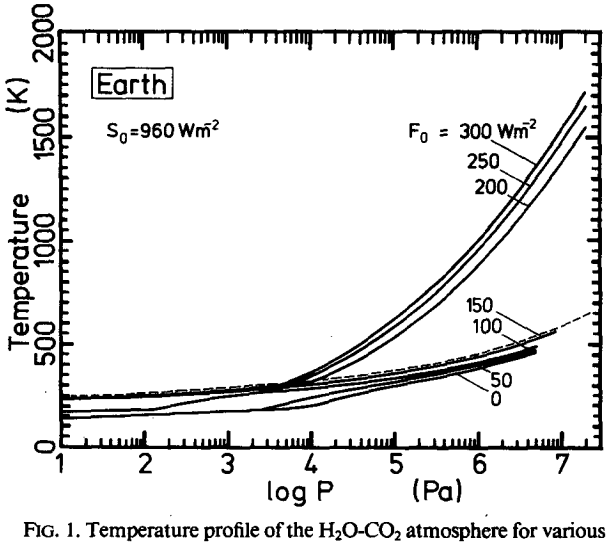

FIG. 1. Temperature profile of the H_2O-CO_2 atmosphere for various F_0 values. Note that the temperature profile for the lower F_0 value is almost along the saturation curve (thin broken curve) of H_2O. Total pressure at the base of the atmosphere changes because of the proto-ocean formation.

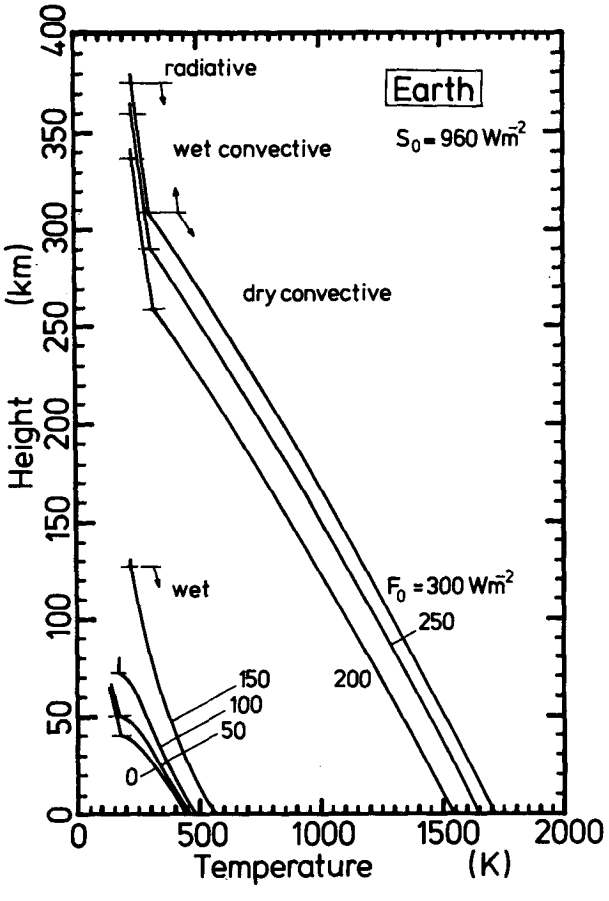

FIG. 2. Vertical temperature profile of the H_2O-CO_2 atmosphere for various F_0 values. When $F_0 \geq 200$ W m^{-2}, height of the tropopause is very high ($\sim$300 km) and the atmospheric structure is divided into three parts: radiative layer, wet-convective layer and dry-convective layer. When $F_0 \leq 150$ W m^{-2}, height of the tropopause decreases to about $\sim$100 km and the dry-convective layer disappears. It implies a proto-ocean formation.

b. H_2O concentration in atmosphere

Figure 3 shows the vertical profile of the H_2O mole fraction in the atmosphere. The broken curve indicates a standard distribution of H_2O in the present tropical atmosphere (McClatchey et al. 1972). The H_2O concentrations in the lower part of the proto-atmosphere are shown to be much larger than that of the present atmosphere. When $F_0 > 150$ W m^{-2}, the atmosphere is almost composed of H_2O. Even when $F_0 = 0$ W m^{-2}, under which conditions the formation of a proto-ocean is possible, the H_2O concentration in the lower atmosphere is much higher than that of the present atmosphere. This is because the surface temperature is much higher than the present value.

When $F_0 < 100$ W m^{-2}, however, H_2O concentration in the upper atmosphere is less than that of the present value. In these cases the temperature structure of the upper atmosphere is not well constrained by our convergence criteria. However, the temperature at the tropopause and below is quite well constrained (within ~1 K). Low H_2O concentration is a consequence of low temperature at the tropopause. If the temperature at tropopause is high, it results in high H_2O concentration, which makes the atmosphere opaque. Then the convective layer extends to the upper atmosphere. It results, then, in low temperature and small concentration of H_2O in the upper atmosphere.

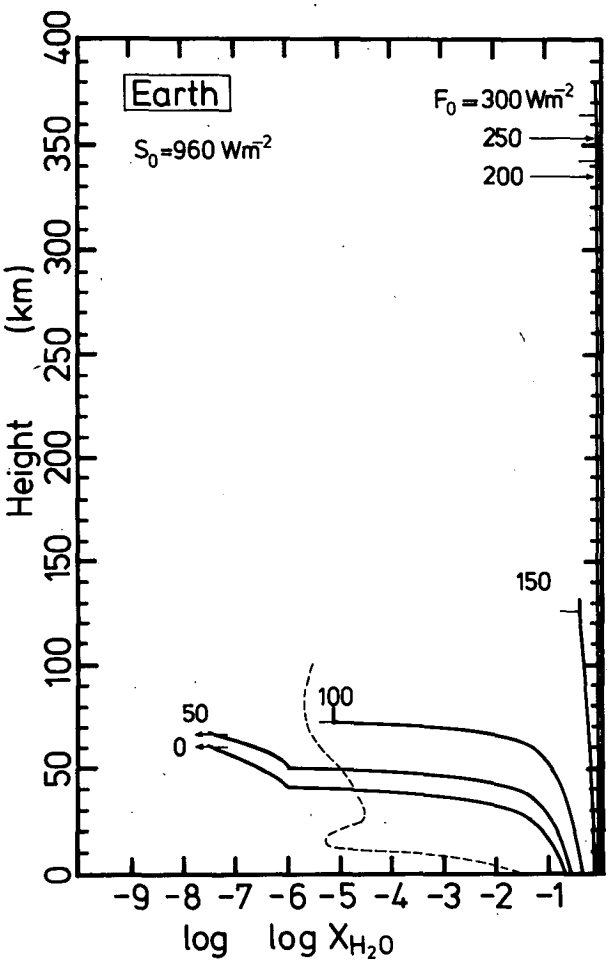

FIG. 3. Vertical distribution of H_2O in the atmosphere. The mole fraction of H_2O is shown for various F_0 values. Tropopause is denoted by a short horizontal bar. Broken curve represents the standard H_2O distribution of the present tropical atmosphere [McClatchey et al. 1972]. Higher stratospheric H_2O concentration is noticed for larger F_0 cases.

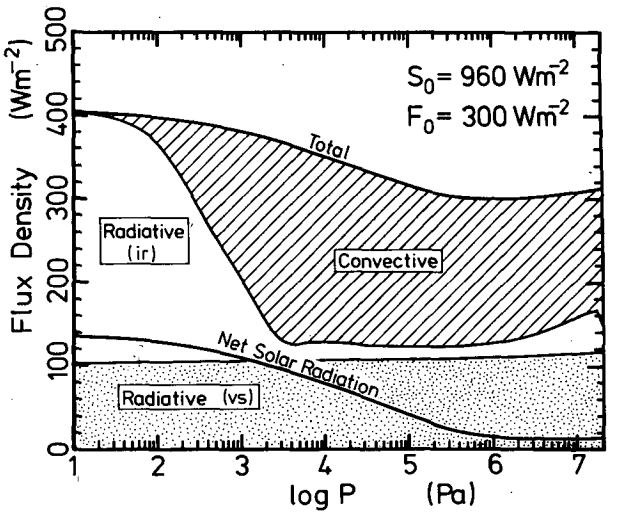

FIG. 4. Vertical distribution of the energy flux density for the case of F_0 = 300 W m^{-2} (E300 model). The total planetary and the net solar flux densities are shown by thick curves. Difference between these two flux densities is the impact energy flux density. The total planetary flux density is divided into three parts: convective (shaded region), net radiant flux density in infrared (<14 286 cm^{-1}, blank region), and the net radiant flux density in visible (>14 286 cm^{-1}, dotted region).

c. Vertical distribution of energy flux density

The vertical profile of radiant flux density for F_0 = 300 W m^{-2} is shown in Fig. 4. In this figure, the total upward energy flux density, convective and net upward radiant flux densities, and the net downward solar radiant flux density are shown. The net upward radiant flux density is divided into those of infrared region (nonscattering bands < 14 286 cm^{-1}) and visible region (scattering bands > 14 286 cm^{-1}).

Net solar radiation decreases with increasing pathlength due to absorption in infrared region (nonscattering bands). Since all the solar radiation in the infrared region is absorbed, it approaches a constant at ~10^6 Pa. The direct solar radiation does not reach the base of the atmosphere even for the visible region (scattering band). Only some amount of diffuse radiation in the scattering band reaches the base of the atmosphere.

The difference between the total and the net solar flux densities is the impact energy flux density given at the surface. At the upper atmosphere ($P < 10^6$ Pa), the total energy flux decreases with increasing pressure owing to the absorption of solar radiation. At the lower atmosphere ($P > 10^6$ Pa), it increases with increasing pressure, because the impact energy flux density increases by the geometrical effect of the spherical atmosphere.

Because of very high surface temperature (1712 K), radiative transfer in the visible region (scattering band $> 14\,286$ cm^{-1}) is very important as a mechanism of upward heat transportation. On the other hand, the radiative transfer in the infrared region (nonscattering bands) is important only at the uppermost layer ($P < 10^3$ Pa). An increase in the radiant flux density in this band with increasing pressure at the lowermost atmosphere is because of the larger lapse rate of these layers.

Figure 5 shows the distribution of the energy flux density for the case of $F_0 = 0$ W m^{-2}. We can see in this figure most of the features previously discussed. In this case, due to low H_2O concentration in the upper atmosphere, absorption of solar radiation begins at slightly higher pressure than in the case of $F_0 = 300$ W m^{-2}. To the contrary, extinction of the direct solar radiation by the Rayleigh scattering begins at slightly lower pressure than that of $F_0 = 300$ W m^{-2}. This is because the scattering cross section of CO_2 is about four times greater than that of H_2O. The low concentration of H_2O in the upper atmosphere also causes an extension of the radiative layer to higher pressure. At the lower atmosphere, however, the radiative transfer in the infrared region is negligible because of the small lapse rate due to wet convection. The upward radiative transfer in the visible region is negligibly small because of the relatively low surface temperature (455 K).

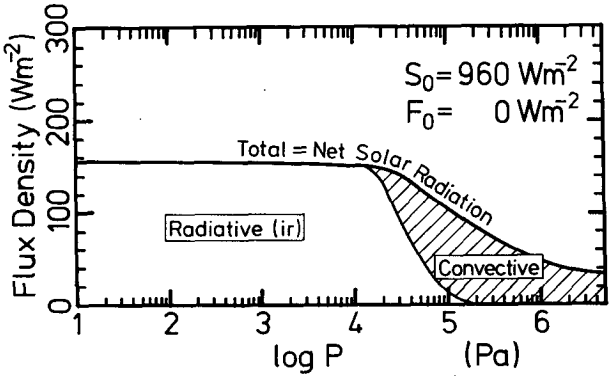

FIG. 5. Vertical distribution of the energy flux density for the case of $F_0 = 0$ W m^{-2} (E0 model). Representations are the same as those of Fig. 4. Note that the net planetary flux density in the infrared region at $P \sim 10^3$ Pa is more efficient than that of $F_0 = 300$ W m^{-2} shown in Fig. 4. This is due to lower H_2O concentration in the upper atmosphere than that of $F_0 = 300$ W m^{-2}. The net planetary flux in the visible region is negligibly small because of relatively low surface temperature.

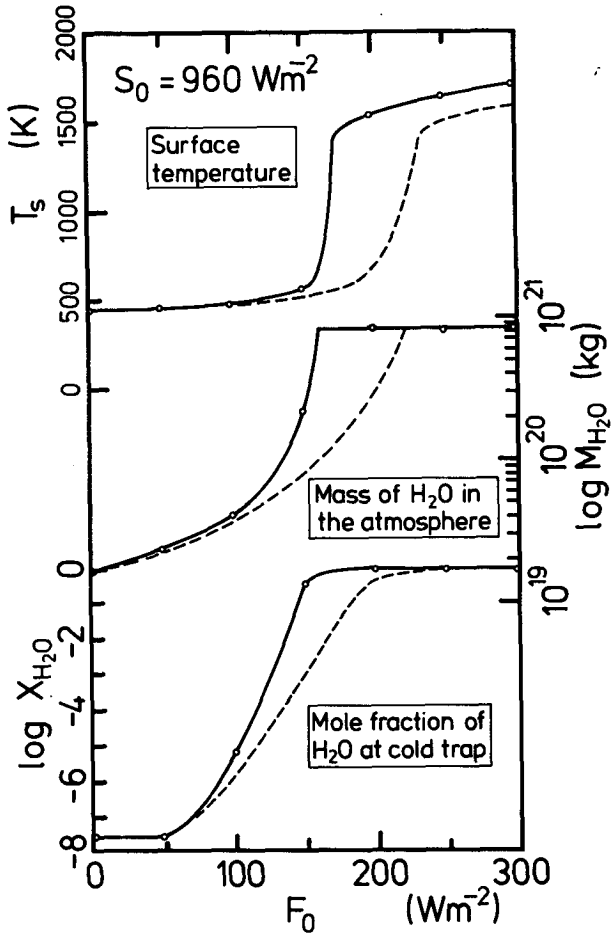

FIG. 6. Variation of the surface temperature, total mass of H_2O in the atmosphere, and mole fraction of H_2O at the cold trap are shown as a function of F_0 (S_0 is fixed at a value of 960 W m^{-2}). All these values change drastically at $F_0 \sim 150$ W m^{-2}. When F_0 becomes smaller than ~ 150 W m^{-2}, a proto-ocean is formed and the surface temperature and mole fraction of H_2O also decrease suddenly.

d. Change in atmospheric structure with F_0

Figure 6 shows the change in surface temperature, total mass of H_2O in the atmosphere and mole fraction of H_2O at the cold trap with changing F_0. Here S_0 is assumed to be 960 W m^{-2}. It is shown that not only the surface temperature and total mass of H_2O in the atmosphere but also the mole fraction of H_2O at the cold trap (the most important parameter on photodissociation of H_2O and subsequent escape of hydrogen) drastically decrease with the formation of a proto-ocean. The change in total mass of H_2O in the atmosphere is closely related to the formation/extinction of a proto-ocean.

It should be noted that the physical meanings of the surface temperature and the total mass of H_2O in the atmosphere is completely different between two cases, $F_0 < \sim 150$ W m^{-2} and $F_0 > \sim 150$ W m^{-2}. For the

cases of $F_0 < \sim 150$ W m^{-2}, liquid and gas phases are in equilibrium at the lower atmosphere. In such a two-components system with two phases, the thermodynamical degree of freedom is 2. Therefore, if we specify F_0 and the mass of CO_2 in the atmosphere, the mass of H_2O in the atmosphere is automatically determined irrespective of the total H_2O inventory. Hence, the results at $F_0 < \sim 150$ W m^{-2} are independent of the total H_2O inventory assumed in this study. On the other hand, for the cases of $F_0 > \sim 150$ W m^{-2}, the lower atmosphere is composed of gas phase only and the degree of freedom is 3. Therefore, the mass of H_2O in the atmosphere is also an independent variable and the results at $F_0 > \sim 150$ W m^{-2} are dependent to an assumed H_2O inventory ($\sim 10^{21}$ kg) in this study. This is similar to the change in atmospheric structure at the critical condition for the runaway greenhouse: once the runaway condition is satisfied, the surface temperature increases until a liquid ocean disappears completely by evaporation. In this respect, $F_0 \sim 150$ W m^{-2} may be considered as a runaway condition for blanketing effect at $S_0 = 960$ W m^{-2} when we consider the change in atmospheric structure with increasing F_0.

Such a change in atmospheric structure is determined by optical properties of H_2O and thermal properties of H_2O and CO_2. Absorption by CO_2 is not important in this structure change. For example, if we neglect the continuum absorption of H_2O outside the "atmospheric window" region (800–1200 cm^{-1}), the critical value of F_0 for structure change increases to about 200 W m^{-2} (broken curves in Fig. 6). However, absorption by CO_2 is not important in this structural change; the change in critical F_0 value is less than 2%, even if we neglect the infrared absorption by CO_2.

4. Discussion

a. Plausibility of assumptions made in the calculation

In this section we discuss the assumptions and simplifications made in this calculation of the atmospheric structure.

1) Optical properties at high pressure and temperature

First we discuss the sensitivity of the results to optical properties at high pressure and temperature where the optical properties are not well understood. In the region where radiative transfer is the dominant mechanism for the energy transfer, the atmospheric structure is significantly affected by its optical properties. As shown in Section 3, however, the radiative transfer is not important as an energy transfer mechanism in the lower atmosphere where the temperature and pressure are high. For example, when $F_0 = 300$ W m^{-2} (Fig. 4), the radiant flux in the infrared region (nonscattering bands) at the lower atmosphere occupies only about one-fourth the convective heat flux. Hence, we may assume that our results are insensitive to the optical properties unless the radiative transfer is enhanced by the effects neglected in the calculation at high pressure and temperature.

Neglecting the temperature dependence of line intensity results in underestimation of the line intensity in the band gap at high temperature, which is more than one order of magnitude at 1500 K (Ludwig 1971). Hence, the absorption in the lower atmosphere is significantly underestimated in this study unless such an increase in the line intensity is completely compensated by the line shape change at high pressure. It implies that the radiative transfer in the lower atmosphere is even less important than considered in this study. In this respect we may conclude that our results are not significantly affected by errors possibly included in the optical data at high temperature and high pressure state such as the line shape change at high pressure and hot bands.

We can also assume that our results are not affected by simplifications made in estimation of the optical properties in the short wavelength range, because the radiation in these spectral ranges is not important for the radiatively equilibrated upper atmosphere.

2) Continuum absorption

The results may be sensitive to possible errors included in the parameterization of the continuum absorption of H_2O, because the continuum absorption covers most of the spectral range of infrared region, which is very important in radiative transfer at low temperature. In addition, the absorption coefficient for the continuum absorption of H_2O increases with increasing H_2O concentration [see Eq. (13)]. Hence the continuum absorption plays a key role in controlling the atmospheric structure of an H_2O-rich atmosphere as pointed by Kasting et al. (1984).

In this study we made the spectral range of continuum absorption as wide as possible. This treatment is different from that of Kasting et al. (1984): for most of their computations Kasting et al. included the continuum absorption only in the "atmospheric window" region from 800–1200 cm^{-1}, where Rodgers and Walshaw (1966) did not derive band-model parameters.

Our treatment of the continuum absorption may give an overestimation of the surface temperature, rather than an underestimation (cf. Kasting et al. 1984), because the line absorption parameters of 6.3 μm band (1200–2200 cm^{-1}) used in this study are based on the total absorption data (Rodgers and Walshaw 1966), and the band parameters include the effect of the continuum absorption. It obviously results in more severe conditions for the proto-ocean formation on the Earth. However, overestimation due to our treatment may not be so significant, because the continuum ab-

sorption is not so large at conditions considered by Rodgers and Walshaw.

If we neglect the continuum absorption outside the window region, as done by Kasting et al. (1984), the critical value of F_0 for proto-ocean formation increases to about 200 W m^{-2} as shown before.

3) Relative humidity and cloud

We assumed that the relative humidity in the atmosphere is 100%. It results in a slight overestimation of the atmospheric temperature. It is, however, difficult to estimate the degree of overestimation caused by this assumption, because we do not know the actual profile of relative humidity distribution in the atmosphere.

One of the most important assumptions made in this study is neglecting cloud. In this section, we try to estimate the effect of cloud at the tropopause by comparing its effects on the net planetary and solar fluxs. Cloud decreases both the net upward planetary flux, L_{pl} and the net solar flux, L_{sl}. However, if decrease of L_{pl} is larger than that of L_{sl}, we may consider that the cloud warms up the atmosphere. The flux L_{pl} may be given as a function of cloudiness c as follows:

$$L_{pl}(c) = L_{irp}(0)[1 - c(1 - f_{irp})] + L_{vsp}[1 - cA_{vs}]$$

where L_{irp} and L_{vsp} are the net upward planetary flux in the infrared and visible regions, respectively. The term A_{vs} is the cloud albedo in the visible region and f_{ir} is a fraction of radiant flux emitted from the stratosphere (higher than the cloud level assumed here). In the derivation of this equation, we assumed the cloud is completely opaque for infrared planetary radiation. Since A_{vs} is less than unity,

$$L_{pl}(c) \geqslant L_{pl}(0) - c[L_{irp}(0)(1 - f_{ir}) + L_{vsp}]. \quad (15)$$

Similarly, L_{sl} is given by

$$L_{sl}(c) = L_{irs}(1 - cA_{ir}) + L_{vss}(1 - cA_{vs})$$

where L_{irs} and L_{vss} are the net solar flux in the infrared and visible regions, respectively. Here A_{ir} is albedo of cloud at infrared region. Usually A_{ir} is smaller than A_{vs}; then,

$$L_{sl}(0) \leqslant L_{sl}(0)(1 - cA_{ir}). \quad (16)$$

For convenience, we define $\Delta L(c) \equiv L_{sl}(c) - L_{pl}(c) + L_0$, where L_0 is the impact energy flux. Since our results give values of $L_{sl}(0)$, and $L_{pl}(0)$ at the equilibrium of no-cloud cases, $\Delta L(0) = 0$. If $\Delta L(c)$ is positive at $c > 0$, cloud warms the atmosphere, and if $\Delta L(c)$ is negative, cloud cools the atmosphere. Since $\Delta L(0) = 0$, $\Delta L(c)$ is given by

$$\Delta L(c) \leqslant c[L_{irp}(0)(1 - f_{ir}) + L_{vsp}(0) - A_{ir}L_{sl}(0)]. \quad (17)$$

From this equation we can see that the cloud warms the atmosphere only if A_{ir} is less than a critical value, $A_{\max} = [(1 - f_{ir})L_{irp}(0) + L_{vsp}(0)]/L_{sl}(0)$. Table 4 shows the values of $L_{pl}(0)$, $L_{sl}(0)$, and f_{ir} calculated in this study, and $A_{\max}$.

For the cases of $F_0 > 0$ W m^{-2}, values of $A_{\max}$ are very large value; if $A_{\max}$ value is larger than 1, the cloud may warm the atmosphere irrespective of its transmittance for solar radiation. Hence, we can assume that the cloud warms up the atmosphere when impact energy is given at the surface and our results give the lower bound of the surface temperature. This is obviously because the impact energy given at the surface is not affected by cloud unlike solar radiation. Such an warming effect of cloud may decrease the critical value of F_0 for proto-ocean formation.

To the contrary, when $F_0 = 0$ W m^{-2} (model E0), a cloud cools the atmosphere unless the transmittance of the cloud for the solar radiation is larger than about 0.5. Transmittance of 500 m-thick stratus cloud with 10 μm diameter drops is estimated to be about 0.66 (Houghton 1977). Judging from very large thickness of the wet-convective layer ($\sim$40 km), much thicker cloud may be more plausible. Therefore, we may conclude that neglecting of cloud results in overestimation of the surface temperature for the case of $F_0 = 0$ W m^{-2}.

We also neglected a silicate cloud possibly formed at lower atmosphere. Its effect may be considered to be similar to that of the H_2O cloud discussed above. Since it is considered to be formed in the lower atmosphere where radiative transfer is not important, its effect may be smaller than that of the H_2O cloud.

TABLE 4. Parameters used for estimation of the effect of cloud.

Model	F_0 (W m^{-2})	L_{pl} (10^{15} W)	L_{sl} (10^{15} W)	L_{irp} (10^{15} W)	L_{vsp} (10^{15} W)	L_{vss} (10^{15} W)	Area (10^{14} m^2)	f_{ir}	$A_{\max}$
E0	0	81.0	80.9	81.0	0.0	16.5	5.21	0.525	0.48
E50	50	107.3	81.2	107.3	0.0	16.8	5.22	0.267	0.97
E100	100	133.3	81.6	133.3	0.0	16.9	5.24	0.186	1.33
E150	150	155.1	77.4	155.1	0.0	11.7	5.33	0.542	0.92
E200	200	179.6	76.7	165.2	14.4	6.6	5.68	0.567	1.12
E250	250	206.0	77.2	168.9	37.1	6.7	5.72	0.549	1.47
E300	300	232.6	77.6	172.6	60.0	6.7	5.74	0.548	1.78

b. Comparison of the results of this study and previous studies

In previous studies (Abe and Matsui 1985, 1986; Matsui and Abe 1986a,b), we have made a number of simplifications in the estimation of the surface temperature during accretion. Here we compare the surface temperature determined in this study with that estimated in the previous papers.

The atmospheric structure was estimated in the previous studies by using the following equation (Abe and Matsui 1985):

$$\sigma T^4 = \frac{1 + \tau^*(P)}{2} F_0 + \frac{S_0}{4} \tag{18}$$

where $\tau^*(P)$ is the effective optical thickness of an impact-generated atmosphere. The term $\tau^*(P)$ for a plane-parallel atmosphere is given by

$$\tau^*(P) = \frac{3}{2} \frac{\bar{\kappa} P}{g} \tag{19a}$$

$$\bar{\kappa} = \left(\frac{\kappa_0 g}{3 P_0} \right)^{1/2} \tag{19b}$$

where κ_0 is the gray absorption coefficient at a reference pressure P_0. The surface temperature, T_s, was thus estimated by

$$\sigma T_s^4 = \frac{2 + \tau^*(P_s)}{2} F_0 + \frac{S_0}{4}. \tag{20}$$

The absorption coefficient of H_2O at ~ 1000 cm^{-1} is adopted as κ_0. Then $\kappa_0 = 0.01$ m^2 kg^{-1} at $P_0 = 101\,325$ Pa (Yamamoto 1952). Though the effect of dry convection was partially taken into account in Eq. (18) (Abe and Matsui 1985), the effect of wet convection, condensation of H_2O, and nonideal behavior of gases were all ignored. Therefore, we need to study uncertainties of the results caused by these crude treatments on the atmospheric structure.

Figure 7 shows the comparison of the atmospheric structure given in this study and that calculated from Eqs. (18) and (19). For the cases of $F_0 < 150$ W m^{-2}, the previous estimate gives higher surface temperature than that given in this study. This is obviously caused by neglecting condensation in the lowering of the lapse rate in the previous method. On the other hand, for the cases of $F_0 > 150$ W m^{-2}, the previous estimate gives a slightly lower temperature ($200 \sim 250$ K) than that given in this study. However, the agreement of these cases is remarkably good judging from a large difference between the two methods. This is because the previous estimate accidentally gives a fairly good approximation of wet-adiabat in the middle atmosphere for high F_0 cases. Underestimation of the surface temperature in these cases is basically due to neglecting the greenhouse effect in Eq. (18). [We use the word "greenhouse" if the atmosphere is heated by solar radiation and use "blanketing" if the atmosphere is heated by energy flux given at the surface (Matsui and Abe 1986b). If $F_0 = 0$, Eq. (18) gives $T_s = (S_0/4\sigma)^{1/4}$ irrespective of optical thickness of the atmosphere. Thus, no "greenhouse" effect is taken into account in Eq. (18); only the "blanketing" effect is considered.]

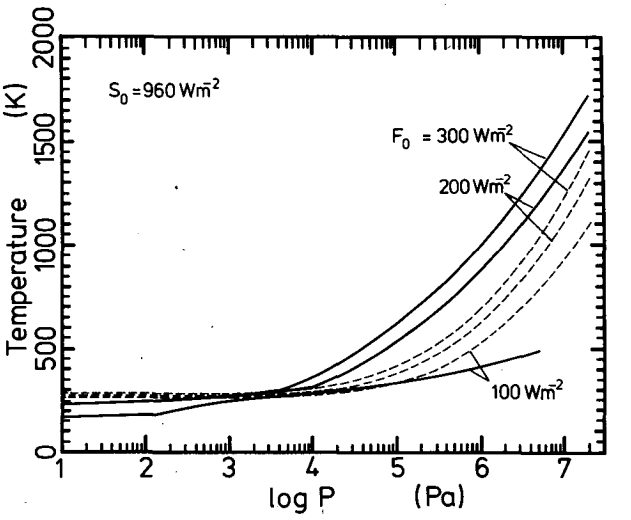

FIG. 7. Radiatively convectively equilibrated atmospheric structures calculated through Eq. (18) (broken curves) are compared with those of a nongray H_2O-CO_2 atmosphere model (solid curves). Three temperature profiles for $F_0 = 300$, 200, and 100 W m^{-2} are shown.

The previous results were, however, shown to be insensitive to the variations in the physical parameters (Abe and Matsui 1986; Matsui and Abe 1986b). In particular, the mass of the atmosphere at the end of accretion is controlled by the existence of a magma ocean. Hence, we may assume that it is not sensitive to the atmospheric structure of low F_0 cases, which is not related to the magma ocean formation. For high F_0 cases, the underestimation of the surface temperature may correspond to underestimation in $\bar{\kappa}$ by a factor of 2. Since the mass of the atmosphere at the end of the accretion is inversely proportional to the square root of $\bar{\kappa}$ (Abe 1986), the difference of $\bar{\kappa}$ by a factor of 2 does not affect an estimate of the mass of an impact-generated atmosphere. Therefore, the previous results are not affected significantly by such an underestimation of the surface temperature. Hence, we can reasonably conclude that the growing Earth had a hot impact-generated atmosphere with about 10^{21} kg of H_2O at the last stage of accretion.

c. Proto-ocean on the proto-earth

1) FORMATION OF A PROTO-OCEAN

As shown in Fig. 6, a proto-ocean is formed once F_0 decreased to ~ 150 W m^{-2}. If we take into account an effect of cloud on the radiative transfer, the resulting

surface temperature is even lower than shown in Fig. 6. Thus, we can conclude that a proto-ocean is formed on the Earth at the last stage of accretion irrespective of the cloudiness. However, the critical value of the impact energy flux (F_0) necessary to cause formation of a proto-ocean may depend on the cloudiness.

The mass of CO_2 in the atmosphere also influences the critical F_0 value. Dependence of F_0 value on the mass of CO_2 will be discussed elsewhere (Abe, personal communication). Qualitatively speaking, a decrease in CO_2 results in decrease in the critical F_0 value, because the decrease of CO_2 increases the net solar radiation by reducing the Rayleigh scattering but not increasing the planetary flux significantly (see section 3d). Then a hot atmosphere is maintained by the solar radiation and a proto-ocean may not be formed until a low F_0 value is reached. However, when the mass of CO_2 is very large and the atmospheric pressure exceeds the critical pressure of H_2O, no liquid water may be formed on the surface of the proto-Earth. At present, it is hard to estimate the evolution of such a proto-atmosphere when the CO_2 mass is larger than the critical value. The surface of the proto-Earth may be entirely covered by high density supercritical fluid composed of H_2O and CO_2 in such a case.

2) Evolution of the atmosphere after the end of accretion

The surface temperature after the end of accretion ($F_0 = 0$ W m^{-2}) is 455 K. The surface temperature of 455 K is still much higher than the present value. It is, however, expected that the surface temperature decreases with decreasing the mass of CO_2 in the atmosphere, since CO_2 gradually dissolves into a proto-ocean and precipitates as carbonates. This is because the lower atmosphere is saturated by water vapor and the surface temperature varies along an adiabat with changing the mass of CO_2 in the atmosphere. This means that the removal rate of CO_2 from the proto-atmosphere determines the decreasing rate of the surface temperature.

Sagan and Mullen (1972) pointed out that the Earth should have been frozen in its early history due to the lower solar luminosity, if it had the present atmosphere. There are many geological observations contrary to the frozen proto-Earth model. Therefore, to prevent the freezing they proposed a rather ad hoc assumption that the proto-atmosphere contained some reducing species. On the other hand, Owen et al. (1979) showed that the CO_2 greenhouse was sufficient to prevent the freezing of the Earth in its early stage of evolution. Our results not only support the results by Owen et al. (1979) but also suggest that the freezing of the Earth is automatically avoided as a consequence of the formation of an impact-generated atmosphere during accretion.

The H_2O might be removed by the photo-dissociation and subsequent escape of hydrogen during the cooling stage of a proto-ocean. It depends on H_2O concentration (X_{H_2O}) in the upper atmosphere. The H_2O concentration at the cold trap is less than 10^{-6} during the cooling stage of a proto-ocean (see Figs. 3 and 6). The mass loss due to the escape of H for such a case is estimated to be less than 10^{11} kg Gy^{-1} under the present day EUV flux by using the escape flux by Kasting and Pollack (1983). This is negligible compared to the mass of H_2O of the ocean, $\sim 10^{21}$ kg. Therefore, we can conclude that the H_2O loss is negligible for the Earth. A similar conclusion is given by Kasting and Ackermann (1986) for a radiatively convectively equilibrated atmosphere with a different composition (present atmospheric composition with enhanced CO_2).

It is interesting to note that the surface temperature ($\sim$400 K) estimated above is very close to the upper limit of estimated temperatures of the archaean ocean. Oskvarek and Perry (1976) estimated the temperature of a proto-ocean based on the oxygen isotope composition of the old (3.8×10^9 yr) chert in Isua metasediments, West Greenland. Their result shows that the upper bound of temperatures of the archaean ocean is between 360 and 420 K. This estimate is dependent on the initial value of isotopic ratio of oceanic water; $\delta^{18}O_{SMOW} = -6$ ppt is appropriate when water is initially equilibrated with igneous material at high temperature. When we adopt this initial value, the estimated temperature is 420 K.

It is not clear whether such a correspondence in the surface temperature indicates the existence of a massive CO_2-rich atmosphere until 3.8×10^9 years ago. Even if this were the case, it does not seem to contradict with the origin of life in the early stage of Earth's evolution. Some kind of archaeobacteria are well known to survive in a high temperature state. Since the escape of atmosphere is negligible, the problem is whether such a long lifetime of the CO_2 atmosphere coexisting with a hot water ocean is possible from the geochemical points of view.

3) Summary

We can summarize an early evolution of the proto-atmosphere on the Earth as follows:

1) a hot proto-ocean is formed on the Earth with decreasing the impact energy at the last stage of accretion;

2) being accompanied with the proto-ocean formation, H_2O concentration in the upper atmosphere decreases, which prevents the photo-dissociation of H_2O in the atmosphere and subsequent escape of hydrogen;

3) at the end of accretion, the surface temperature of the proto-Earth is about 400 K which is consistent with the observational estimate based on the archaean chert (3.8×10^9 yr old); and

4) the surface temperature goes down gradually with

decreasing CO_2 in the atmosphere due to a geochemical reaction between water and CO_2. Hence, we could show without any ad hoc assumption that an impact-generated atmosphere evolves to the present atmosphere.

d. Implications on the early evolution of Venus

The present atmosphere of Venus contains only a very small amount of H_2O. However, the deuterium-hydrogen (D/H) ratio measured by Pioneer-Venus mass spectrometer ($(1.6 \pm 0.2) \times 10^{-2}$; Donahue et al. 1982) is 105 times larger than that of the Earth. It indicates that the initial abundance of H_2O in the Venusian atmosphere is, at least, 0.14% of the present terrestrial H_2O.

In the previous study we have shown that the mass of an H_2O atmosphere on Venus at the end of accretion is similar to that of the Earth ($\sim 10^{21}$ kg) (Matsui and Abe 1986c). This conclusion was derived from a calculation similar to that for the Earth by Abe and Matsui (1986) and Matsui and Abe (1986b), in which the greenhouse effect was not taken into account as discussed before. In addition, by using a simple radiative equilibrium model, in which the greenhouse effect was taken into account, we also concluded that no ocean was formed on a proto-Venus because of large solar radiation (Matsui and Abe 1986c). However, since no convection was taken into account in the previous greenhouse model, it is still an interesting problem whether a proto-ocean formed on a proto-Venus or not.

By using the method developed in this study we calculate the structure of an H_2O–CO_2 atmosphere on a proto-Venus by assuming the mass and the radius of the planet to be the same as those of the Earth. The vertical temperature profile of a proto-Venusian atmosphere at the end of accretion ($F_0 = 0$ W m^{-2}) is shown in Fig. 8. In this calculation, the masses of H_2O and CO_2 in the atmosphere are assumed to be 10^{21} kg and $\sim 3 \times 10^{20}$ kg, respectively. (See Table 3 for model parameters and results). The calculated temperature profile is similar to that of the Earth's model with F_0 = 150 W m^{-2} (E150 model; Fig. 2) and the surface temperature is 535 K. Unlike the conclusion by Matsui and Abe (1986c) a proto-ocean is formed even on Venus in this case. This is obviously because of the effect of the wet convection which was not taken into account in the previous calculation.

Since clouds lower the surface temperature when no impact energy flux is given at the surface ($F_0 = 0$ W m^{-2}), we may conclude that a proto-ocean formed on Venus at the end of accretion irrespective of the cloud cover, if H_2O and CO_2 inventories of the proto-Venus were similar to those of the Earth ($M_{H_2O} \sim 10^{21}$ kg, and $M_{CO_2} \sim 5 \times 10^{20}$ kg).

On the other hand, if the H_2O inventory of a proto-Venus is much smaller than that of the present Earth,

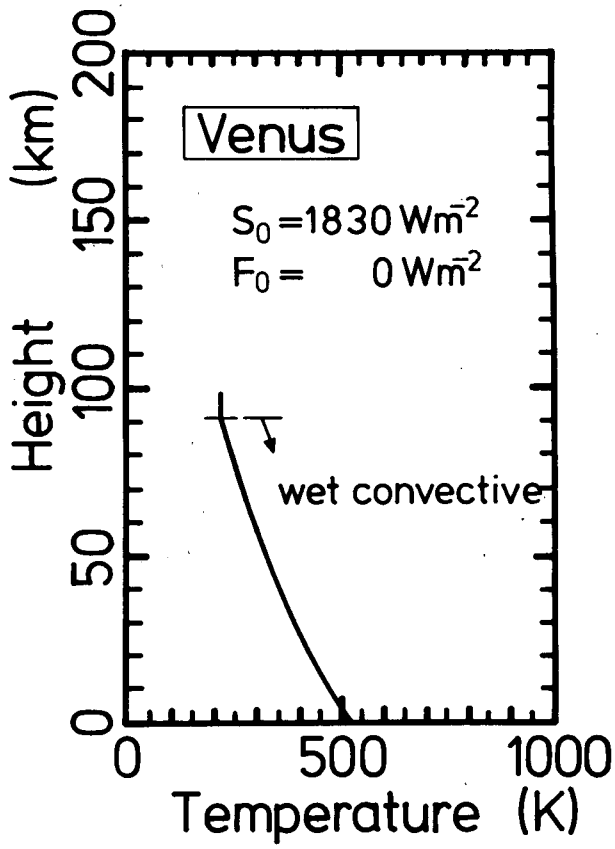

FIG. 8. Vertical temperature profile of a proto-Venusian H_2O-CO_2 atmosphere. The atmospheric structure is similar to that of the E150 models, (F_0 = 150 W m^{-2} in Fig. 2).

a proto-ocean might not be formed on Venus. As shown in Table 3, our model atmosphere of proto-Venus contains about 10^{20} kg of H_2O. It implies that all H_2O on a proto-Venus should be kept in the atmosphere and no proto-ocean could form on the surface, if the atmospheric inventory of H_2O on a proto-Venus was smaller than about 10^{20} kg. Unlike our previous conclusion, the H_2O inventory could be smaller than that value, because our previous estimation (Matsui and Abe 1986c) is possibly an overestimation owing to neglecting the greenhouse effect. Thus, whether a water ocean was formed on a proto-Venus or not is critically dependent on the H_2O inventory in the proto-atmosphere.

Some information on the H_2O inventory of the proto-Venus may come from the discussions on the loss of H_2O from Venus. It has been discussed by many authors (McElroy et al. 1981; Watson et al. 1981; Kasting and Pollack 1983; Kumer et al. 1983; Kasting et al. 1984; Richardson et al. 1984; Krasnopolsky 1985) based on a runaway greenhouse of the proto-Venusian atmosphere proposed by Ingersoll (1969): the runaway greenhouse makes the H_2O concentration in the upper atmosphere high, then H_2O is easily lost due to the

photo-dissociation and lost by subsequent escape of hydrogen (Brinkmann 1969). When the dissociation rate of H_2O is large, hydrogen may be lost by hydrodynamic escape. This process was extensively studied by Kasting and Polack (1983). They showed that a mass of H_2O comparable to the terrestrial ocean could be lost by this mechanism during Venusian history. Even during the existence of a proto-ocean, loss of H_2O would occur, as discussed by Kasting et al. (1984), because the concentration of H_2O in the upper atmosphere is expected to be high (see Table 3).

However, it has been pointed out that if proto-Venus had 90 bar of CO_2-rich atmosphere and $\sim 10^{21}$ kg of proto-ocean, the D/H ratio in the present atmosphere should be higher than the observed value (Kasting and Pollack 1983; Krasnopolsky 1985). This is because the D/H ratio rapidly increases at the final stage of hydrodynamic escape with decreasing H_2O concentration in the upper atmosphere (e.g., Kasting and Pollack 1983). This may suggest that the H_2O inventory of a proto-Venus was much smaller than that of the Earth. Krasnopolsky (1985) concluded that an H_2O inventory of about 1% of the terrestrial ocean ($\sim 10^{19}$ kg) seemed to be more probable on the proto-Venus. Although it is not clear why the H_2O inventory was so small if this was the case, a proto-ocean may not be formed as discussed before.

As another possibility, however, Kasting et al. (1984) showed that, if CO_2 accumulation occurred after the dissipation of H_2O, the initial water mass comparable to that of the terrestrial ocean is consistent with the observed D/H ratio. This is because H_2O concentration in the upper atmosphere is kept very high (~ 1) when the mass of the noncondensable gas (CO_2) is small. A high H_2O concentration is maintained while a proto-ocean exists on the surface of Venus. It results in a high escape rate of hydrogen and thus the D/H ratio is not affected significantly.

In this case the problem is why the CO_2 accumulation occurred after the dissipation of water. Kasting et al. (1984) argued that CO_2 might be tied up in the near-surface layers as carbonate while water ocean existed. However, this seems difficult because a small amount of CO_2 can not yield the high surface temperature required for dissociation of carbonate (cf. Rasool and deBergh 1970). Although carbonates might be possibly dissociated owing to subduction of the lithosphere and degas into the atmosphere by volcanism, it is not clear whether or not a plate tectonics existed on Venus. In addition, a low $^{40}Ar/^{36}Ar$ ratio in the present Venusian atmosphere may also indicate low efficiency of degassing after the end of accretion on Venus.

In summary, a proto-ocean is formed at the end of accretion, if the proto-Venusian atmosphere contains a similar amount of H_2O as the Earth. In this case, judging from the D/H ratio, the amount of CO_2 in the proto-Venusian atmosphere must be kept smaller than the present value during loss of H_2O by some mechanism. Then, the problem is how CO_2 accumulated after the loss of H_2O. On the other hand, if the H_2O inventory of the proto-Venusian atmosphere was about 1% of the terrestrial value, as suggested from D/H ratio, no ocean would be formed. In this case, the problem is why the H_2O inventory of the proto-Venus was so small compared to the terrestrial value. Hence, further study on the atmosphere formation during accretion and a possible style of carbon recycling on a proto-Venus is required to discuss the formation of a water ocean on Venus.

Acknowledgments. This is a part of the D.Sc. thesis of one of the authors (Y.A.) submitted to the University of Tokyo. Y.A. appreciates Professor T. Matsuno's comments on the structure of an H_2O-rich atmosphere at the early stage of this study. A revised manuscript was prepared while Y.A. was at the California Institute of Technology. He is grateful to Professor A. P. Ingersoll for his critical comments on the manuscript. Numerical calculations were performed mainly by M-280H and M-682H at the Computer Centre of the University of Tokyo and partly by MX-3000 at the Geophysical Institute. A terminal program "ETERM" developed by K. Takano and K. Kohketsu was used on PC9800. This research was partly supported by a Grant-in-Aid for encouragement of young scientists (No. 62790137) sponsored by the Ministry of Education, Science, and Culture of Japan.

Note Added In Proof. Similar calculation on a hypothetical steam atmosphere was also independently done by Kasting (1988) using a different method. Numerical results of his and our studies seem to agree very well in spite of the different methods.

APPENDIX A

Calculation of the Radiative Flux of a Thick and Nongray Atmosphere

1. Thermal radiation in nonscattering bands

Consider a nonscattering and plane-parallel atmosphere which is in local thermodynamic equilibrium. Since we consider fairly large number of spectral bands, we may reasonably assume that radiation is monochromatic in each band.

$$F_k(u) = \int_{u_t}^{u_b} \frac{d\pi B_k(u')}{du'} T_{RFk}(|u' - u|)du' + \pi[B_{bk} - B_k(u_b)]T_{RFk}(u_b - u) + \pi[B_k(u_t) - B_{tk}]T_{RFk}(u - u_t) \quad \text{(A1)}$$

where u is the mole number in a vertical column with a unit area. Here u is defined by

$$u = \int_z^\infty n(z)dz \quad \text{(A2)}$$

where $n(z)$ is the mole density of atmospheric gas and

u_b and u_t are the u values at the base and top of the atmosphere, respectively; T_{RFk} is the slab transmission function for the kth spectral band defined by

$$T_{RFk}(u_1 - u_2) \equiv 2\int_0^1 T_{Rk}(u_1, u_2, \mu)\mu d\mu, \quad (u_1 < u_2) \tag{A3}$$

where $T_{Rk}(u_1, u_2, \mu)$ is the column transmission function between levels u_1 and u_2 for radiation toward the zenith angle θ and $\mu = \cos\theta$. For band absorption, T_R is given either by Fels' (1979) formula or the Howard et al. (1956) empirical formula. For continuum absorption, T_R is given by Eq. (13). In the derivation of Eq. (A1) we assumed that irradiations at the top and base of the atmosphere are the black body radiation.

Now we divide the atmosphere into $N_l + 1$ layers defined by atmospheric pressure. In this study we set N_l to be 50. The pressure at the top of the uppermost layer is assumed to be $10^{-6}P_s$, where P_s is the pressure at the base of the atmosphere. In each layer $d\pi B/du$ is assumed to be constant. Then the net upward radiant flux density, F_{kj}, for the kth spectral interval at the midpiont of the jth layer is given by

$$F_{kj} = \sum_{i=1}^{N_l-1}\left(\frac{d\pi B_k}{du}\right)_i \int_{u_i}^{u_{i+1}} T_{RFk}(|u' - \hat{u}_j|)du' + \pi[B_{k1} - B_{kt}]T_{RFk}(\hat{u}_j - u_1) + \pi[B_{kb} - B_{kN_l}]T_{RFk}(u_{N_l} - \hat{u}_j) \tag{A4}$$

where u_i is the u value at the ith level and $\hat{u}_j$ is the u value at the midpoint of the jth layer. We define T_{RFkji} and $(dB/dU)_{kj}$ as follows

$$T_{RFkji} = \begin{cases} \displaystyle\int_{u_i}^{u_{i+1}} T_{RFk}(|u' - \hat{u}_j|)du', \\ \qquad\qquad (i = 1, \cdots, N_l - 1) \\ T_{RFk}(\hat{u}_j - u_1), \quad (i = 0) \\ T_{RFk}(u_{N_l} - \hat{u}_j), \quad (i = N_l) \end{cases} \tag{A5}$$

$$(dB/dU)_{kj} \equiv \begin{cases} \pi(B_{k,j+1} - B_{k,j})/(u_{j+1} - u_j), \\ \qquad\qquad (j = 1, \cdots, N_l - 1) \\ \pi(B_{k,1} - B_{kt}), \quad (j = 0) \\ \pi(B_{kb} - B_{k,N_l}), \quad (j = N_l). \end{cases} \tag{A6}$$

Here T_{RFkji} is determined by the numerical integration of Eq. (A5) using the Curtis–Godson approximation and the discrete ordinate method with the order 3. The integration step was determined so that the maximum normal optical distance which corresponds to the integration step may be smaller than 0.2 (Kasting et al. 1984). The numerical integration is carried out within the region where normal optical distance from the midpoint of the jth layer is smaller than 10. For the optically very thick atmosphere, T_{RFkji} $(j \neq i)$ are negligibly small but T_{RFkji} $(j = i)$ are always nonzero. Then we can calculate the radiant flux density even for the thick atmosphere as precisely as for the thin atmosphere. This method is similar to that used by Pollack (1969) and Kasting et al. (1984) but more direct, because we use $d\pi B/du$ instead of the temperature gradient.

Then the net upward radiant flux density, F_{irj}, integrated over all the nonscattering bands at jth layer is given by

$$F_{irj} = \sum_k \sum_{i=0}^{N_l} T_{RFkji}(dB/dU)_{ki}$$

$$F_{irj} = \sum_{i=0}^{N_l} T_{RFji}(dB/dU)_i \tag{A7}$$

where

$$T_{RFji} \equiv \begin{cases} \displaystyle\sum_k G_{ki}\int_{u_i}^{u_{i+1}} T_{RFk}(|u' - \hat{u}_j|)du', \\ \qquad\qquad (i = 1, \cdots, N_l - 1) \\ \displaystyle\sum_k G_{ki}T_{RFk}(\hat{u}_j - u_1), \quad (i = 0) \\ \displaystyle\sum_k G_{ki}T_{RFk}(u_{N_l} - \hat{u}_j), \quad (i = N_l) \end{cases} \tag{A8}$$

$$(dB/dU)_j \equiv \begin{cases} \pi(B_{j+1} - B_j)/(u_{j+1} - u_j), \\ \qquad\qquad (j = 1, \cdots, N_l - 1) \\ \pi(B_1 - B_t), \quad (j = 0) \\ \pi(B_b - B_{N_l}), \quad (j = N_l). \end{cases} \tag{A9}$$

G_{ki} is defined by

$$G_{ki} \equiv \begin{cases} (dB/dU)_{ki}/(dB/dU)_i & (B_{i+1} \neq B_i) \\ B_i/B_{ki} & (B_{i+1} = B_i). \end{cases} \tag{A10}$$

If we set B_t to be 0 in Eq. (A7), F_{ir} represents the thermal radiation from the atmosphere. Equation (A7) can be used for the calculation of the radiatively equilibrated atmospheric structure.

2. Solar radiation in nonscattering bands

Since the solar zenith angle varies with latitude, it is difficult to determine a representative value for the solar zenith angle averaged over the entire planet. Hence we treated the solar radiation at the top of the atmosphere as a diffuse radiation for simplicity. Then the solar radiation in the kth nonscattering band is given by

$$F_{slkj} = \sum_k \pi B_{kt}T_{RFk}(u_j - u_1)$$

$$F_{slkj} = \sum_k \pi B_{kt}T_{RFkj0}. \tag{A11}$$

We determine B_t so that the following relation may hold

$$\frac{S_0}{4} = \sum_k^{all} \pi B_{kt} \quad \text{(A12)}$$

where B_{kt} is assumed to be proportional to the black body radiation at 5970 K.

3. Radiative-convective equilibrium

In the following, we describe how to determine the atmospheric structure in radiative-convective equilibrium. First, we guess the surface temperature for a given set of physical quantities at the base of the atmosphere: atmospheric pressure, mole fraction of H_2O at the surface, energy flux density, and solar flux density. As an initial condition, we assume the temperature profile to be adiabatic and calculate at first the radiant flux of such an atmosphere.

A condition required for the radiative equilibrium is given by

$$4\pi r^2 F_{irp}(r) = 4\pi r^2 [F_{irs}(r) + F_{vss}(r)] - L_{vsp}(r) + 4\pi r_0{}^2 F_0 \quad \text{(A13)}$$

where F_{irp} and F_{irs} are the net upward thermal and downward solar flux densities in the non-scattering bands, respectively, and L_{vsp} and F_{vss} are the net upward radiation flux and downward flux densities of direct solar radiation in the scattering band, respectively. Since we assume a perfect scattering in the scattering band, L_{vsp} does not depend on the vertical temperature profile of the atmosphere. Then the right-hand side of the equation does not depend explicitly on the temperature profile of the atmosphere. Hence we can determine a deviation of thermal flux density, dF_{irp}, from the radiative equilibrium.

Once dF_{irp} is given, we can calculate the correction, $d(dB/dU)_i$, of $(dB/dU)_i$ by solving Eq. (A7). Iterating such a procedure we can easily estimate the radiatively equilibrated temperature profile. The procedure of the convective adjustment is similar to that used by Kasting et al. (1984). The difference between this study and previous studies is that we use dB/dU instead of temperature gradient dT/dz.

The convergence criterion for the radiative equilibrium is assumed to be $|dF_{irp}| < 0.01|F_{irp}|$. Though one may consider this criterion to be too loose, more severe criteria are nonsensical because the precision of the equation of state itself is a few percent. In a convective layer, where the temperature gradient is given by the adiabatic one, the convergence criterion is given by $dF_{irp} > -0.01|F_{irp}|$. This is because the radiative transfer is not efficient and dF_{irp} may be positive in the convective layer.

In this calculation we use the pressure grid as a vertical coordinate. We do not give any constraint on the total mass of the atmosphere. This is a rather important point in calculating a structure of an atmosphere mainly composed of condensable gas, because selection of another grid system may result in numerical instability during the iteration: if we use a grid system defined by the height or the cumulative mass, the pressure on a grid point changes slightly during iteration due to change in temperature profile. Such a slight change in pressure results in a large unexpected change in the temperature profile, which may result in numerical instability in the calculation. Such an instability was noticed by Kasting et al. (1984). For example, a few milibar change at the top of the wet region may result in 1000 K change at the base of the atmosphere ($\sim$200 bar). This situation may be understood as follows: when only a condensable gas composes the system, the equilibrium between vapor and condensed phases is achieved along the saturation vapor pressure. It means that in the atmosphere composed mainly of a condensable gas, any wet-adiabat should be very close to the saturation curve irrespective of its molar entropy. To the contrary, the dry-adiabat, which determines the temperature of the lower convective atmosphere, varies with its molar entropy. Hence, a small change in temperature and pressure in the wet region results in a large change in temperature profile of the lower atmosphere. If we use a pressure grid, the pressure on the grid point does not change in iteration process. Then, by using the method described above, we can calculate the change of temperature at the base of the atmosphere caused by the change of temperature in the upper atmosphere.

APPENDIX B

Wet-Adiabat for Condensable and Nonideal Gas Mixture

We derive an adiabatic temperature gradient for the gas-cloud (ice or liquid water) mixture system. We consider a small parcel, composed of n_v moles of condensable gas, n_i moles of noncondensable gas component i, and n_c moles of condensable gas component in cloud particles. The total mole number of the gas phase is thus represented by $n_g \equiv n_v + \sum_i n_i$. Henceforth, the subscripts v, i, g, and c denote the condensable gas, ith noncondensable gas, total gas phase, and cloud particle, respectively: for example, C_{vi} represents the heat capacity with constant volume per unit mole of ith noncondensable gas. For simplicity, we assume that 1) the entropy of the parcel is given by the sum of that of gas phase and cloud particles, 2) cloud particles are composed of pure H_2O, and 3) cloud particles are in equilibrium with gas phase. Then the entropy of the parcel, S, is given by

$$S(P, T, n_v, n_i, n_c) = n_g s_g(P, T, n_v, n_i) + n_c s_c(P, T) \quad \text{(B1)}$$

where s_g and s_c are the entropy of the gas phase and cloud particles per unit mole, respectively.

A condition required for equilibrium between cloud particles and condensable gas is given by

$$\Delta g(P, T, n_v, n_i) \equiv \mu_c(P, T) - \mu_v(P, T, n_v, n_i) = 0 \quad \text{(B2)}$$

where μ_c and μ_v are the chemical potential of condensable gas (H_2O) in the gas phase and cloud particles, respectively. The wet adiabat is derived by solving the following equations:

$$dS = 0 = \left(\frac{\partial S}{\partial T}\right)_{P,n_v,n_i} dT + \left(\frac{\partial S}{\partial P}\right)_{T,n_v,n_i} dP + \left(\frac{\partial S}{\partial n_v}\right)_{P,T,n_i} dn_v \quad \text{(B3)}$$

$$d\Delta g = 0 = \left(\frac{\partial \Delta g}{\partial T}\right)_{P,n_v,n_i} dT + \left(\frac{\partial \Delta g}{\partial P}\right)_{T,n_v,n_i} dP + \left(\frac{\partial \Delta g}{\partial n_v}\right)_{P,T,n_i} dn_v. \quad \text{(B4)}$$

Thus, the wet-adiabat is given by

$$\left(\frac{\partial T}{\partial P}\right)_s = \frac{S_n G_p - S_P G_n}{S_T G_n - S_n G_T} \quad \text{(B5)}$$

$$\left(\frac{\partial n_v}{\partial P}\right)_s = n_g \frac{S_P G_T - S_T G_P}{S_T G_n - S_n G_T} \quad \text{(B6)}$$

with

$$S_T \equiv \frac{1}{n_g}\left(\frac{\partial S}{\partial T}\right) \quad \text{(B7a)}$$

$$S_P \equiv \frac{1}{n_g}\left(\frac{\partial S}{\partial P}\right) \quad \text{(B7b)}$$

$$S_n \equiv \left(\frac{\partial S}{\partial n_v}\right) - \left(\frac{\partial S}{\partial n_c}\right) \quad \text{(B7c)}$$

$$G_T \equiv \frac{\partial \Delta g}{\partial T} \quad \text{(B7d)}$$

$$G_p \equiv \frac{\partial \Delta g}{\partial P} \quad \text{(B7e)}$$

$$G_n \equiv n_g \frac{\partial \Delta g}{\partial n_v}. \quad \text{(B7f)}$$

We can calculate the wet-adiabat if the above partial derivatives are given. In general, the entropy of gas-phase per unit mole is given by

$$s_g(P, T, n_v, n_i) = \sum_j \frac{n_j}{n_g}\left[s^I_{j0}(T) - R \ln\left(\frac{n_j P}{n_g P_0}\right)\right] - \int_0^P \left[\left(\frac{\partial v}{\partial T}\right)_P - \frac{R}{P'}\right] dP' \quad \text{(B8)}$$

where summations are taken for all gas species in the system, including condensable gas. (In general, integrals with pressure represent deviations from ideal gas or effects of nonzero volume of condensed phase.) Here s^I_{j0} is defined by

$$s^I_{j0}(T) \equiv \int_{T_0}^T \frac{C^I_{pj0}(T')}{T'} dT'.$$

The chemical potential of water vapor in a gas mixture is given by

$$\mu_v(P, T, n_v, n_i) = g^I_{v0} + RT \ln \frac{n_v P}{n_g P_0} + \int_0^P \left[v_v - \frac{RT}{P'}\right] dP' \quad \text{(B9)}$$

where

$$g^I_{v0}(T) \equiv \int_{T_0}^T C^I_{pv0}(T') dT' - T s^I_{v0}(T).$$

The entropy and chemical potential of cloud particles are calculated by the following procedure. At saturation vapor pressure, $P^*(T)$, of pure condensable gas, the cloud particles are in equilibrium with pure condensable gas. Then the chemical potential of cloud particles is expressed by

$$\mu_c(P^*(T), T) = \mu^*_v(P^*(T), T)$$

$$\mu_c(P^*(T), T) = g^I_{v0}(T) + RT \ln \frac{P^*(T)}{P_0} + \int_0^{P^*(T)} \left[v^*_v - \frac{RT}{P'}\right] dP' \quad \text{(B10)}$$

where μ^*_v and v^*_v are the chemical potential and the molar volume of pure condensable gas. [Henceforth the superscript asterisk indicates "pure" material, except for the saturation vapor pressure $P^*(T)$]. By taking into account the pressure effect, the chemical potential of cloud particles at pressure, P, is given by

$$\mu_c(P, T) = g^I_{v0}(T) + RT \ln \frac{P^*(T)}{P_0} + \int_0^{P^*(T)} \left[v^*_v - \frac{RT}{P'}\right] dP' + \int_{P^*(T)}^P v^*_c \, dP'. \quad \text{(B11)}$$

Then, the entropy of cloud particles is given by

$$s_c(P, T) \equiv -\left(\frac{\partial \mu_c}{\partial T}\right)_P$$

$$s_c(P, T) = s^I_{v0} - R \ln \frac{P}{P_0} - \int_0^P \left[\left(\frac{\partial v^*_v}{\partial T}\right)_{P'} - \frac{R}{P'}\right] dP' + \frac{\partial}{\partial T}\int_{P^*(T)}^P (v^*_v - v^*_c) dP' \quad \text{(B12)}$$

Δg is thus

$$\Delta g(P, T, n_v, n_i) = -RT \ln \frac{n_v}{n_g} - \int_0^P (v_v - v^*_v) dP' - \int_{P^*(T)}^P (v^*_v - v^*_c) dP'. \quad \text{(B13)}$$

The partial derivatives are given by

$$S_T = \left[\left(\frac{n_v}{n_g} + \frac{n_c}{n_g}\right)\frac{C^I_{pv0}}{T} + \sum_i \frac{n_i}{n_g}\frac{C^I_{pi0}}{T}\right] - \int_0^P \left(\frac{\partial^2 v_g}{\partial T^2}\right) dP' - \frac{n_c}{n_g}\int_0^P \left(\frac{\partial^2 v^*_v}{\partial T^2}\right) dP' + \frac{n_c}{n_g}\frac{\partial^2}{\partial T^2}\int_{P^*(T)}^P [v^*_v - v^*_c] dP' \quad \text{(B14a)}$$

$$S_P = -\left[\left(\frac{\partial v_g}{\partial T}\right) + \frac{n_c}{n_g}\left(\frac{\partial v^*_c}{\partial T}\right)\right] \quad \text{(B14b)}$$

$$S_n = -R \ln \frac{n_v}{n_g} - \int_0^P \left[\left(\frac{\partial v_v}{\partial T}\right) - \left(\frac{\partial v^*_v}{\partial T}\right)\right] dP' - \frac{\partial}{\partial T}\int_{P^*(T)}^P [v^*_v - v^*_c] dP' \quad \text{(B14c)}$$

$$G_T = S_n \quad \text{(B14d)}$$

$$G_p = -v_v + v^*_c \quad \text{(B14e)}$$

$$G_n = -RT\left(\frac{n_g}{n_v} - 1\right) - n_g \int_0^P \left(\frac{\partial v_v}{\partial n_v}\right)_{n_i} dP'. \quad \text{(B14f)}$$

We can rewrite the above equations by using the mole fraction relative to the gas phase, x_v, x_i, and x_c, defined by

$$x_v \equiv n_v/n_g, \quad x_i \equiv n_i/n_g, \quad x_c \equiv n_c/n_g. \quad \text{(B15)}$$

Hence, the partial derivatives of the mole fraction with respect to the mole number of condensable gas in the system are

$$\left(\frac{\partial x_v}{\partial n_v}\right)_{n_i} = \frac{(1 - x_v)}{n_g} \quad \text{(B16a)}$$

$$\left(\frac{\partial x_i}{\partial n_v}\right)_{n_i} = -\frac{x_i}{n_g} \quad \text{(B16b)}$$

$$\left(\frac{\partial x_c}{\partial n_v}\right)_{n_i} = -\frac{1 + x_c}{n_g}. \quad \text{(B16c)}$$

Then, the gradient of mole fraction along the wet-adiabat is given by

$$\left(\frac{\partial x_v}{\partial P}\right)_s = (1 - x_v)\frac{S_p G_T - S_T G_P}{S_T G_n - S_n G_T} \quad \text{(B17a)}$$

$$\left(\frac{\partial x_i}{\partial P}\right)_s = -x_i \frac{S_p G_T - S_T G_P}{S_T G_n - S_n G_T} \quad \text{(B17b)}$$

$$\left(\frac{\partial x_c}{\partial P}\right)_s = -(1 + x_c)\frac{S_p G_T - S_T G_P}{S_T G_n - S_n G_T}. \quad \text{(B17c)}$$

Thus, equilibrium condition and partial derivatives are expressed by Eqs. (1)–(4) in text.

A wet-adiabat exists only when $\Delta g = 0$. If $\Delta g > 0$, H_2O vapor does not condense into ice or liquid water. To get a dry-adiabat given by Eqs. (6) and (7), put $n_c = dn_c = 0$ in Eqs. (B3) and (B14) and solve them. We also get a pseudo-adiabat in a similar way; putting n_c equal to 0 in Eqs. (B3), (B4), and (B14).

To calculate an adiabatic temperature gradient from these equations, we need to determine at first the molar volume of gas phase at a given temperature, pressure and mole fraction of water vapor. We also need to calculate the molar volume of pure condensable gas (water vapor) and cloud particles at saturation pressure. Using the partial molar volume, we can evaluate Δg. If Δg is positive, no condensation occurs in the atmosphere. Then a dry-adiabatic temperature gradient is calculated from Eq. (6). If Δg is negative, condensation occurs in the atmosphere. Then the mole fraction of water vapor, x_v, at equilibrium is determined by using the bisection method, and a wet-adiabat is calculated from Eq. (1). In this case we assumed that the gas-cloud particle mixture contains cloud particles less than 1% of its bulk density. These procedure starts from the base of the atmosphere toward the top. Hence, the mole fraction of water vapor in the upper atmosphere is always smaller than that of the lower atmosphere whenever condensation occurs in the atmosphere. A minimum value of the mole fraction is given at the highest point where condensation occurs, i.e., the cold trap.

APPENDIX C

Estimation of Band Parameters at Short Wavelength

To estimate the band parameters of a band "gap", we use the laboratory data compiled by Ferriso et al. (1966) and its revised version by Ludwig (1971). They parameterized the column transmission by using two parameters, k and a: $S/\delta \equiv k$ and $\pi\alpha_L/\delta \equiv 4a$. The parameter k is tabulated by Ludwig (1971) for the wavenumber range 0–9300 cm^{-1} with a 25 cm^{-1} spectral interval. The parameter a is given by γ/d (Ferriso et al. 1966), where γ and d are half-width and mean line spacing, respectively. In their parameterization, γ

is assumed to be only a function of pressure. Then γ is given by

$$\gamma = \sum_i P_i \gamma_i \,(\text{atm})(273/T\,(\text{K}))^{1/2} + \gamma^*_{H_2O} P_{H_2O}(273/T\,(\text{K})) \quad \text{(C1)}$$

where P_i is the partial pressure of gas component i, and $\gamma^*_{H_2O}$, γ_{H_2O} and γ_{CO_2} are assumed to be 0.44, 0.12 and 0.09, respectively. For the air at STP condition, γ is given to be 0.08.

As a consequence of their assumption, the frequency dependence of nondimensional line width a is included in d. However, they did not give any specific d values. Instead, only a mean value of d averaged over all frequencies, $\bar{d}$, was given by Ferriso et al. (1966); $\bar{d}$ was given by

$$\bar{d} = \exp(1.21 - 0.00106T\,(\text{K})). \quad \text{(C2)}$$

At STP condition, $\bar{d} = 2.51$. Since no other data can be obtained, we use the values of $\bar{d}$ and γ for H_2O in the air at STP condition. Then a is estimated to be 3.19×10^{-2} over all the frequency intervals. It corresponds to $\pi\alpha_{L0}/\delta = 0.1276$.

It is not clear whether we can use an average value of $\pi\alpha_{L0}/\delta$ as a representative value for wide range of wavelength. Howard et al. (1956) showed that their absorption data for vibration-rotation bands of H_2O can be fitted by one general transmission function. It may imply that we can use the above $\pi\alpha_{L0}/\delta$ value as a value representing rather a wide range of wavelength. Hence, we use $\pi\alpha_{L0}/\delta = 0.1276$ in this study.

We use an average of the mean of k and harmonic mean of k in the given spectral bands as the S/δ values. For shorter wavelength range, however, Ludwig (1971) did not compile k values (>9300 cm^{-1}). Then we need to estimate the S/δ value by extrapolation from longer wavelength data. The log$k$ values at the bottom of the band gap decreases linearly with increasing wavenumber; this dependence may be expressed by $k \approx 0.68^{k_w}$, where k_w is the wavenumber in cm^{-1}. We use this relation to estimate the S/δ values for the spectral bands at 9300–10 100, 11 500–11 906, and 12 658–13 514 cm^{-1}.

Fowle (1915) measured the total absorption under the Earth's atmospheric condition for 0.81 and 0.7 μm bands of H_2O. We estimate the S/δ values for the spectral bands at 11 906–12 658 and 13 514–14 286 cm^{-1} based on the Fowle's data. Though these data cover only small absorption (less than 20%), we tried to fit them using the Goody random model. The term $\pi\alpha_{L0}/\delta$ was assumed to be 0.1276.

Absorption by CO_2 at 750–1200 cm^{-1} was not parameterized by Rodgers and Walshaw (1966). This absorption does not play an important role in an H_2O-rich atmosphere, because the continuum absorption of H_2O is much stronger than these absorption. However, to obtain a better result for less H_2O-rich atmospheres, we parameterized them based on band parameters tabulated by Houghton (1977) by using a similar method to H_2O.

REFERENCES

Abe, Y., 1986: Early evolution of the terrestrial planets: accretion, atmosphere formation, and thermal history. D.Sc. thesis, University of Tokyo, 113, Japan.

——, and T. Matsui, 1985: The formation of an impact-generated H_2O atmosphere and its implications for the early thermal history of the earth. *Proc. Lunar Planet. Sci. Conf. 15th, J. Geophys. Res.*, **90**, C545–C559.

——, and ——, 1986: Early evolution of the Earth: accretion, atmosphere formation, and thermal history. *Proc. Lunar Planet. Sci. Conf. 17th, J. Geophys. Res.*, **91**, E291–E302.

Allen, C. W., 1963: *Astrophysical Quantities, 2nd. ed.* University London Press, 291 pp.

Bignell, K. J., 1970: The water-vapor infra-red continuum. *Quart. J. Roy. Meteor. Soc.*, **96**, 390–403.

Boslough, M. B., R. J. Weldon and T. J. Ahrens, 1980: Impact induced water loss from serpentine, nontronite, and kernite. *Proc. Lunar Planet. Sci. Conf. 11th, Geochim. Cosmochim. Acta*, suppl. 14, 2145–2158.

——, T. J. Ahrens, J. Vizgirda, R. H. Becker and S. Epstain, 1982: Shock-induced devolatilization of calcite. *Earth Planet. Sci. Lett.*, **61**, 166–170.

Brinkmann, R. T., 1969: Dissociation of water vapor and evolution of oxygen in the terrestrial atmosphere. *J. Geophys. Res.*, **74**, 5355–5368.

Brown, H., 1952: Rare gases and formation of the earth's atmosphere. *The Atmospheres of the Earth and Planets*, G. P. Kuiper, Ed., revised edition, University Chicago Press, 258–266.

Burch, D. E., and D. A. Gryvnak, 1966: Laboratory investigation of the absorption and emission of infrared radiation. *J. Quant. Spectrosc. Radiat. Transfer*, **6**, 229–240.

Donahue, T. M., J. H. Hoffman, R. R. Hodges and A. J. Watson, 1982: Venus was wet: A measurement of the ratio of deuterium to hydrogen. *Science*, **216**, 630–633.

Eisenberg, D., and W. Kauzmann, 1969: *The structure and properties of water.* Oxford, 302 pp.

Ezer, D., and A. G. W. Cameron, 1965: A study of solar evolution. *Can. J. Phys.*, **43**, 1497–1517.

Fels, S. B., 1979: Simple strategies for inclusion of Voigt effects in infrared cooling rate calculations. *Appl. Opt.*, **18**, 2634–2637.

Ferriso, C. C., C. B. Ludwig and A. L. Thomson, 1966: Empirically determined infrared absorption coefficients of H_2O from 300 to 3000°K. *J. Quant. Spectrosc. Radiat. Transfer*, **6**, 241–273.

Fowle, F. E., 1915: The transparency of aqueous vapor. *Astrophys. J.*, **42**, 394–411.

Goody, R. M., 1964: *Atmospheric radiation I, theoretical basis.* Oxford University Press, London, 436 pp.

Hamano, Y., and M. Ozima, 1978: Earth–atmosphere evolution model based on Ar isotopic data. *Terrestrial rare gases*, E. C. Alexander and M. Ozima, Eds., Center for Academic Publ. Japan, Tokyo, 155–177.

Hougen, O. A., K. M. Watson and R. A. Ragatz, 1959: *Chemical process principles*, part II, 2nd ed., Wiley.

Houghton, J. T., 1977: *Physics of the Atmospheres.* Cambridge University Press, 203 pp.

Howard, J. N., D. E. Burch and D. Williams, 1956: Infrared transmission of synthetic atmospheres. *J. Opt. Soc. Amer.*, **46**, 186–190, 237–241, 242–245, 334–338, 452–455.

Ingersoll, A. P., 1969: The runaway greenhouse: A history of water on Venus. *J. Atmos. Sci.*, **26**, 1191–1198.

Jakosky, B. M., and T. J. Ahrens, 1979: The history of an atmosphere of impact origin. *Proc. Lunar Planet. Sci. Conf. 10th, Geochim. Cosmochim. Acta*, suppl. 11, 2727–2739.

Kastling, J. F., 1988: Runaway and moist greenhouse atmospheres and the evolution of Earth and Venus. *Icarus*, **74**, 472–494.

——, and J. B. Pollack, 1983: Loss of water from Venus. I. Hydrodynamic escape of hydrogen. *Icarus*, **53**, 479–508.

——, and T. P. Ackerman, 1986: Climatic consequences of very high carbon dioxide levels in the earth's early atmosphere. *Science,* **234,** 1383–1385.

——, J. B. Pollack and T. P. Ackerman, 1984: Response of Earth's atmosphere to increase in solar flux and implications for loss of water from Venus. *Icarus,* **57,** 335–355.

Keenan, J. H., F. G. Keyes, P. G. Hill and J. G. Moore, 1978: *Steam tables, thermodynamic properties of water including vapor, liquid, and solid phases (international system of units—S.I.).* Wiley and Sons.

Kondratyev, K. Y., 1969: *Radiation in the atmosphere.* Academic Press, 912 pp.

Krasnopolsky, V. A., 1985: Total injection of water vapor into the Venus atmosphere. *Icarus,* **62,** 221–229.

Kumar, S., D. M. Hunten and J. B. Pollack, 1983: Nonthermal escape of hydrogen and deuterium from Venus and Implications for loss of water. *Icarus,* **55,** 369–389.

Lange, M. A., and T. J. Ahrens, 1982a: The evolution of an impact-generated atmosphere. *Icarus,* **51,** 96–120.

——, and ——, 1982b: Impact induced dehydration of serpentine and the evolution of planetary atmospheres. *Proc. Lunar Planet. Sci. Conf. 13th, J. Geophys. Res.,* **87,** A451–A456.

——, and ——, 1984: FeO and H_2O and the homogeneous accretion of the earth. *Earth Planet Sci. Lett.,* **71,** 111–119.

——, and ——, 1986: Shock-induced CO_2 loss from $CaCO_3$. *Earth Planet. Sci. Lett.,* **77,** 409–418.

Ludwig, C. B., 1971: Measurements of the curves-of-growth of hot water vapor. *Appl. Optics.,* **10,** 1057–1073.

McClatchey, R. A., R. W. Fenn, J. E. A. Selby, F. E. Volz and J. S. Garing, 1972: Optical properties of the atmosphere. 3rd ed., *AFCRL Envirm. Res. Rep.,* **411,** 108 pp.

McElroy, M. B., M. J. Prather and J. M. Rodoriguez, 1981: Escape of hydrogen from Venus. *Science,* **215,** 1614–1615.

Matsui, T., and Y. Abe, 1986a: Formation of a "magma ocean" on the terrestrial planets due to the blanketing effect of an impact-induced atmosphere. *Earth Moon Planets,* **34,** 223–230.

——, and ——, 1986b: Evolution of an impact-induced atmosphere and magma ocean on the accreting earth. *Nature,* **319,** 303–305.

——, and ——, 1986c: Impact-induced atmosphere and oceans on Earth and Venus. *Nature,* **322,** 526–528.

Newman, M. J., and R. T. Rood, 1877: Implications of solar evolution for the Earth's early atmosphere. *Science,* **198,** 1035–1037.

Oskvarek, J. D., and E. C. Perry, 1976: Temperature limits on the early archaean ocean from oxygen isotope variations in the Isua supracrustal sequence, West Greenland. *Nature,* **259,** 192–194.

Owen, T., R. D. Cess and V. Ramanathan, 1979: Enhanced CO_2 greenhouse to compensate for reduced solar luminosity on early Earth. *Nature,* **277,** 640–642.

Peng, D.-Y., and D. B. Robinson, 1976: A new two-constant equation of state. *Ind. Eng. Chem. Fundam.,* **15,** 59–64.

Poldervaart, A., 1955: Chemistry of the Earth's crust. *Crust of the Earth (Geol. Soc. Amer. Spec. Pap., 62),* A. Poldervaart, Ed., 119–144.

Pollack, J. B., 1969: A nongrey CO_2-H_2O greenhouse model of Venus. *Icarus,* **10,** 314–341.

——, 1971: A Nongray calculation of the runaway greenhouse: Implications for Venus' past and present. *Icarus,* **14,** 295–306.

——, and Y. L. Yung, 1980: Origin and evolution of planetary atmosphere. *Annual Review of Earth Planetary Sciences,* **8,** 425–487.

Rasool, S. I., and C. DeBergh, 1970: The runaway greenhouse and the accumulation of CO_2 in the Venus atmosphere. *Nature,* **226,** 1037–1039.

Richardson, S. M., J. B. Pollack and R. T. Reynolds, 1984: Water loss on Venus: The role of carbon monoxide. *Icarus,* **60,** 307–316.

Roach, W. T., 1961: The absorption of solar radiation by water vapour and carbon dioxide in a cloudless atmosphere. *Quart. J. Roy. Meteor. Soc.,* **87,** 364–373.

Roberts, R. E., J. E. A. Selby and L. M. Biberman, 1976: Infrared continuum absorption by atmospheric water vapor in the 8–12-μm window. *Appl. Optics,* **15,** 2085–2090.

Rodgers, C. D., and C. D. Walshaw, 1966: The computation of infrared cooling rate in planetary atmosphere. *Quart. J. Roy. Meteor. Soc.,* **92,** 67–92.

Sagan, C., and G. Mullen, 1972: Earth and Mars: Evolution of atmospheres and surface temperatures. *Science,* **177,** 52–56.

Saito, S., 1983: *Fundamentals of equilibrium property estimation* (in Japanese). Revised ed., Baifu-kan, 276 pp.

Walker, J. C. G., 1975: Evolution of the atmosphere of Venus. *J. Atmos. Sci.,* **32,** 1248–1256.

Watson, A. J., T. M. Donahue and J. C. G. Walker, 1981: The dynamics of a rapidly escaping atmosphere: Applications to the evolution of Earth and Venus. *Icarus,* **48,** 150–166.

——, —— and W. R. Kuhn, 1984: Temperatures in a runaway greenhouse on the evolving Venus: Implications for water loss. *Earth Planet. Sci. Lett.,* **68,** 1–6.

White, K. O., W. R. Watkins, C. W. Bruce, R. E. Meredith and F. G. Smith, 1978: Water vapor continuum absorption in the 3.5–4.0-μm region. *Appl. Optics,* **17,** 2711–2720.

Yamamoto, G., 1952: On a radiation chart. *Sci. Rep. Tohoku University,* Ser. 5, *Geophysics,* **14,** 9–23.